Control Engineering Practice 141 (2023) 105724

Contents lists available at ScienceDirect

Control Engineering Practice

journal homepage: www.elsevier.com/locate/conengprac

Real-time predictive model for reactivity controlled compression ignition marine engines

Xiaoguo Storm [a,*], Aneesh Vasudev [a], Amir-Mohammad Shamekhi [a], Amin Modabberian [b], Kai Zenger [b], Jari Hyvönen [c], Maciej Mikulski [a,d,*]

[a] School of Technology and Innovation, Energy Technology, University of Vaasa, Wolffintie 32, FI-65200 Vaasa, Finland
[b] School of Electrical Engineering, Aalto University, Maarintie 8, FI-00076, Espoo, Finland
[c] Wärtsilä Finland Oy, Frilundintie 7, FI-65170 Vaasa, Finland
[d] Vaasa Energy Business and Innovation Centre (VEBIC), Yliopistonranta 1, FI-65200 Vaasa, Finland

ARTICLE INFO

Keywords:
Low-temperature combustion
RCCI
Multi-zone model
Real-time model
Model predictive control

ABSTRACT

Model-based design is proven to be essential for the development of control systems. This paper presents a real-time predictive control-orientated model (COM) for low-temperature combustion (LTC), dual-fuel, reactivity-controlled compression ignition (RCCI) engines. A comprehensive model-based design methodology must be capable of constructing an RCCI control-orientated model with high accuracy, high noise immunity, good response, predictivity in governing mechanisms, and low computation time. This work attains all of these for the first time for a cutting-edge RCCI marine engine. The real-time model (RTM) captures the key sensitivities of RCCI by controlling the total fuel energy and the blend ratio (BR) of two fuels, while also considering uncertainties arising from variations of inlet temperature and the gas exchange process. It provides not only the cycle-wise combustion indicators but also the crank-angle-based cylinder pressure trend. The RTM is derived by direct linearisation of a physics-based model and is successfully validated against experimental results from a large-bore, RCCI engine and the previously acknowledged UVATZ (University of Vaasa Advanced Thermo-kinetic Multi-zone) model. Validation covers both steady-state and transient modes. With high accuracy in several case studies representing typical load transients and air-path disturbance rejection tests, the model predicts maximum cylinder pressure (P_{max}), crank-angle of 5 % burnt (CA5), crank-angle of 50 % burnt (CA50) and indicated mean effective pressure (IMEP) with root means square (RMS) errors of 8.6 %, 0.3 %, 0.6 %, and 0.6 % respectively. The average simulation time without any code optimisation is around 5 ms/cycle, offering sufficient real-time surplus to incorporate a semi-predictive emission submodel within the current approach.

1. Introduction

Low temperature combustion concepts are a novel group of technologies (Agarwal et al., 2017) that enable internal combustion engine (ICE) powertrains to achieve ultra-low emissions of nitrogen oxides (NOx) and particulate matter (PM) while simultaneously improving thermal efficiency, beyond current commercially applied combustion strategies. This is by virtue of lower combustion temperatures (<1800 K) and lean mixtures (Stanglmaier & Roberts, 1999). Amongst many LTC concepts (Dempsey et al., 2014), popularly homogeneous charge compression ignition (HCCI), partially premixed combustion (PPC), etc., RCCI has emerged as superior (Reitz & Duraisamy, 2015). This is due to over a 4 percentage points (pp) improvement in break thermal efficiency over contemporary technology (Hanson et al., 2016), and NOx and PM emissions within EURO VI emission limits (Jia & Denbratt, 2015) achieved without aftertreatment system. RCCI is currently on the agenda of the combustion engine research community, where The University of Wisconsin Madison (Reitz & Duraisamy, 2015), FEV (Dahodwala et al., 2015), CMT Motores Termicos (Benajes et al., 2015; García Valladolid et al., 2017) TU-Eindhoven/TNO (Mikulski et al., 2016; Xia et al., 2019) and some Finnish universities (Ahmad et al., 2019; Kahila et al., 2019; Mikulski, Balakrishnan et al., 2019, Mikulski, Ramesh et al., 2019) are amongst those driving the concept towards real-world applications. The individual research groups are backed by strategic collaborations with major heavy-duty truck and marine original equipment manufacturers. being a dual fuel engine, RCCI combines premixed low reactivity fuel (LRF), such as gasoline, with early direct-injected (DI) high-reactivity

* Corresponding authors at: School of Technology and Innovation, Energy Technology, University of Vaasa, Puuvillakuja 8, FI-65200 Vaasa, Finland.
E-mail addresses: xiaoguo.storm@uwasa.fi (X. Storm), maciej.mikulski@uwasa.fi (M. Mikulski).

https://doi.org/10.1016/j.conengprac.2023.105724
Received 29 June 2023; Received in revised form 20 September 2023; Accepted 22 September 2023
Available online 9 October 2023

Nomenclature and abbreviations

ANN	artificial neural network
BR	blend ratio
CAD	crank angle degree
CAX	crank angle of X % mass burnt
CFD	computational fluid dynamics
COM	control-orientated model
CHR	cumulative heat release
DI	direct injection
DF	dual fuel
EIL	engine in the loop
EVC	exhaust valve closure
EGR	exhaust gas recirculation
HCCI	homogeneous charge compression ignition
HIL	hardware-in-the-loop
HRF	high-reactivity fuel
HRR	heat release rate
ICE	internal combustion engine
IMEP	indicated mean effective pressure
IVC	inlet valve closing
LRF	low-reactivity fuel
LTC	low-temperature combustion
LFO	light fuel oil
LNG	liquified natural gas
MIL	model-in-the-loop
MPC	model predictive control
MVM	mean value model
MZM	multi-zone model
NG	natural gas
NO_X	oxides of nitrogen
PPC	partially premixed combustion
PM	particulate matter
RTM	real-time model
PRR	pressure rise rate
RCCI	reactivity-controlled compression ignition
RMS	root means square
SCRE	single-cylinder research engine
SOC	start of combustion
SOI	start of injection
SSM	state-space model
TDC	top dead centre
UVATZ	University of Vaasa Advanced Thermo-kinetic Multi-zone

Notation and description

a	defined tuneable coefficient
A	cylinder area
B	cylinder bore
br_{change}	monotony transition point
D_x	gradient parameter of X to control input
ΔX	change of X
γ	ratio of specific heats
h_c	convection coefficient
λ	relative air/fuel ratio
M_{gas}	gas fuel mass
M_{egr}	EGR mass ratio
M_{diesel}	diesel fuel mass
E_{fuel}	total fuel energy
P_{cyl}	in-cylinder pressure
P_{IVC}	inlet valve closing pressure
P_{max}	maximum cylinder pressure
$dQ_c/d\theta$	heat-release rate
$dQ_{ht}/d\theta$	heat-transfer rate
LHV_{gas}	gas fuel lower heating value
LHV_{diesel}	diesel fuel lower heating value
Q_c	accumulated heat released
S	SOC shifting parameter
T_{int}	intake-manifold temperature
T_{IVC}	inlet valve closing temperature
T_W	wall-surface temperature
T_{exh}	exhaust temperature
θ_{IVC}	inlet valve closing timing
T_{IVC}	inlet valve closing volume
U	system input
V	cylinder volume
V_d	displacement volume

fuel (HRF) such as diesel. The ensuing combustion is kinetically controlled chemical auto-ignition. This phenomenon is extremely sensitive to in-cylinder conditions, ranging from fuel blending, and mixture formation to thermal- and compositional-stratification, thus highly non-linear in response. The well-known challenges of RCCI include high-load operation being typically limited by excessive peak pressures and steep pressure rise rates (Dempsey et al., 2014); while low-load operation (natural gas fuelling), afflicted by poor combustion performance, resulting in high levels of methane (CH_4) and CO emissions. Therefore, RCCI incorporates several sophisticated subsystems to control combustion. These may include high-pressure fuel injection (multi-pulse) (Molina et al., 2015), variable geometry or sequential turbocharging (Taghavifar et al., 2021) variable valve actuation (Mikulski et al., 2018), or on-board fuel reforming (Mikulski et al., 2019). Currently, there are 12 to 15 independently-controlled parameters (Atkinson, 2014), and Fig. 1 illustrates the burden on traditional controller calibration.

Thus, model-based controller development paradigm is required to save time and cost (Paykani et al., 2021). However, the approach applied to RCCI development, necessitates a high-quality COM. Such a model must offer predictivity in governing mechanisms, accuracy, high noise immunity, good response and low computation time (Dong et al., 2017). Usually, these criteria cannot be met simultaneously, so different models based on their computation time (Rajasingham, 2021) can be

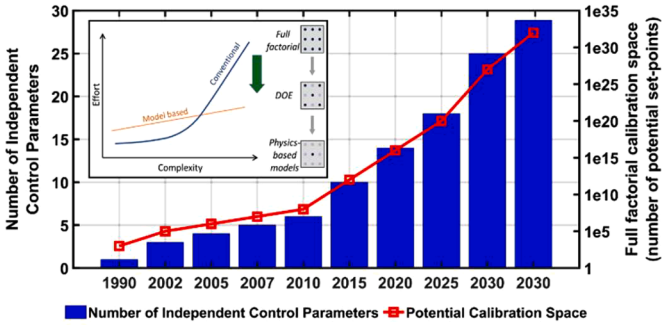

Fig. 1. Engine calibration space showing the exponential increase in the calibration burden as the number of independent control parameters increase. (reproduced from the work of Atkinson (Atkinson, 2014).With permission from the ELSEVIER (Vasudev et al., 2022b).

used in two possible methods. An offline COM is used to design and validate the controller, whereas an online or RTM is integrated into the on-board controller as a digital twin of the physical system.

An offline predictive COM is a reduced-order, phenomenological model, able to accurately represent governing physics, such as the

influence of changes in inlet valve closing (IVC) on combustion phasing and heat release profile. For LTC applications, these models are typically chemical-kinetics based, while making simplifications about secondary-level phenomena like in-cylinder flows (Vasudev et al., 2022b). These physics-based approaches enable flexibility beyond engine- and fuel-specific properties and are not restrained by size of the training dataset (Raut et al., 2018). Recently, Vasudev et al. (2022a) raised the state-of-the-art in thermo-kinetics-based COM, including the ability to predict in-cylinder pressure within cycle-to-cycle variation, with a simulation time of just a few minutes per engine cycle. Because reaction kinetics are accurately represented, the trend-wise predictivity of emissions is inherent with this approach. As such, fast, yet fully predictive multi-zone models (MZM) are a valuable part of model-based development workflow, as elaborated in Vasudev et al. (2022b), by reducing calibration effort/time for sophisticated control systems (Fig. 1) required by such RCCI/LTC engines. On the other hand, to achieve near real-time simulation speeds, offline COMs like MZM are not suitable. Although computational expense can be lowered by reducing modelling fidelity by methods, such as simplified reaction schemes (Mikulski et al., 2015a, 2015b) or absences of reaction kinetics (Guardiola et al., 2018; Kakoee et al., 2020; Khodadadi & Shahbakhti, 2016; Raut et al., 2018; Sui et al., 2020), this can render the models into a data-driven approach. This limits a COM's scalability, mode-switching capability and operating range. Thus, with the necessity of fidelity, computation speed and accuracy in mind, Table 1 summarises the different realisations of real-time-capable COM for LTC applications.

Although their governing phenomena are similar, RCCI and PPC usually have more control parameters than HCCI. Consequently, RCCI and PPC are more challenging to model, as illustrated by the colour-coding used in Table 1 to indicate the level of challenge. Hu et al. (2022); Turesson (2018); Turesson et al. (2018), for instance, assumed up to three multi-pulse injections to shape the heat release in their PPC concept. They introduced seven additional fuel-related control parameters: three for the start of injection (SOI), three for injection duration and one for injection pressure. An RCCI COM (Basina et al., 2020; Irdmousa et al., 2019; Raut et al., 2018) also needs to capture the fuel reactivity characterised by the BR between injected high- and low-reactivity surrogates. Control-orientated modelling of fully-homogenous compression ignition, on the other hand, usually involves two or three inputs, as seen in models by Norouzi et al. (2019); Ebrahimi (2016); Ebrahimi et al. (2016); Ebrahimi and Koch (2015, 2018). Note, however, that complexity is further influenced by the level of sophistication of the airpath control. Norouzi et al. (2019) included only exhaust valve closure (EVC) as a relevant input, whereas studies by Mikulski et al. (2019) and Indrajuana et al. (2018) used fully variable valve actuation to increase the degrees of freedom.

An abundance of control parameters means that not all of them can be captured in real-time simulations, so it is typical for a COM to either limit the number of influential variables, based on a sensitivity analysis (Ebrahimi et al., 2016; Norouzi et al., 2019), or to combine direct control actuator signals to higher-level physical parameters that can be sensed in the engine or estimated with separate virtual sensors (Jeyamoorthy et al., 2022; Kakati et al., 2019; Scocozza et al., 2021). This reduction needs to be considered both on the input and response sides. To this end, Norouzi et al. (2019) and Irdmousa et al. (2019) considered only the main combustion indicators like CA50, IMEP, and maximum pressure rise rate (PRR), arguing that their time-invariant data-driven model can hardly provide high frequency in-cycle combustion details. Excelling over such mean-value approaches, Turesson et al. (2018) and Hu et al. (2022) used a physics-based approach to reproduce in-cylinder pressure and emissions (NOx and/or PM) according to crank angle. This gave high estimation accuracy in all aspects, and a direct understanding of the physics process, which predigests the calibration work, thus needing less amount of data. Furthermore, their physics-based COM had

Table 1
Summary of the RTM in LTC engine model predictive control development. Colour coding: green –stronger in the category; yellow – intermediate ranking; red – weaker in the category.

Reference	*Norouzi (2019)* (Norouzi et al., 2019)	*Turesson (2018)* (Turesson, 2018)	*Hu et al. (2022)* (Hu et al., 2022)	*Raut (2018)*(Raut et al., 2018)	*Irdmousa (2019)* (Irdmousa et al., 2019)	***Present work***
Combustion Concept	HCCI B=97mm 1-cyl	PPC B=130mm 6-cyl (Heavy-duty)	PPC B=126mm 1-cyl	RCCI B=86mm 4-cyl	RCCI B=86mm 4-cyl	RCCI B=310mm 1-cyl (marine)
RTM Approach	▪Combustion: *physics-based MVM* (time invariant SSM)	▪Combustion: *physics-based Pcyl model* ▪Emission: *empirical NO_X \ T_{exh} model*	▪Combustion: *P_{cyl} model (linearised Wiebe)* ▪Emission: *back-propagation ANN*	▪Combustion: *linearised quasi-empirical MVM* (time invariant SSM)	▪Combustion: *Data-driven linear parameter varying (LPV) SSM*	▪Combustion: *physics-based P_{cyl}* (linearised MVM, time varying SSM)
System Variables	2-var. *fuel energy, EVC*	6-var. *SOI* x3, *fuel energy*	4-var. *SOI* x2, *inj.dur* x2	3-var. *fuel energy, BR, SOI*	3-var. *fuel energy, BR, SOI*	2-var. *fuel energy, BR* *disturbances: T_{int} & M_{egr}*
System Feedback	*CA50, IMEP*	P_{cyl} (CAD) CA50, IMEP, P_{max} NO_X , T_{exh}	P_{cyl} (CAD) CA50, IMEP NO_X , PM	P_{cyl} (CAD) *CA50, IMEP*	CA50	P_{cyl} (CAD) CA50, IMEP
RTM Accuracy	$AVGe_{CA50}$ = 1.2CAD	e_{CA50} = 1CAD* e_{IMEP} = 1bar* $AVGe_{Pmax}$ = 2.5bar $MAXe_{NOx}$ = 22.5%	$MAXe_{CA50}$ = 9% $MAXe_{IMEP}$ = 4.7% $AVGe_{NOx}$ = 5% $AVGe_{PM}$ = 5%	$AVGe_{CA50}$ = 1.8CAD $AVGe_{IMEP}$ = 0.36bar	$AVGe_{CA50}$ = 1CAD	$RMSe_{CA50}$ = 0.6% $RMSe_{CA5}$ = 0.3% $RMSe_{IMEP}$ = 0.6% $RMSe_{Pmax}$ = 8.6%
Simulation Speed	Real-time 6.4ms (in-cycle) CPU i7 2.66 GHz	real time 50ms (90% time spent on NOx model)	Real-time 0.35ms (1/100 cycle) CPU i7-7700HQ @2.8GHz	Real-time (in-cycle)	Real-time (in-cycle)	Real-time 5ms (in-cycle) CPU i7-11850H @2.5GHz
Validation	MIL (Detailed Physical Model)	HIL (LabVIEW EIL)	MIL (Potential for MPC)	HIL (dSPace)	HIL (dSPace)	MIL (Potential for MPC)

*The MPC controller tracking error.

P_{cyl} = cylinder pressure; AVGe = average error; MAXe = maximum error; CAD=crank angle degree; inj.dur = injection duration; EGR= exhaust gas recirculation; M_{egr}=EGR mass ratio; T_{int}=Intake-manifold temperature;EIL= engine in the loop; SSM= state-space model;.

a wide operating range and ultra-high computation speed, reported to be just 1 % of the engine cycle time (without emission submodels). The authors provided proof of concept in hardware-in-loop (HIL) simulation, verifying the applicability of their approach in real-world control.

The above-mentioned physics-based COM by the Lund University group (Turesson et al. (2018) and Hu et al. (2022)) establishes the fidelity of LTC COM affording a wide range of predictive control functions. However, although inspirational, the approach taken by both these two studies was designed for multi-injection, single-fuel PPC strategies. They benefit from good controllability provided by triggering injection near TDC, giving relatively linear combustion characteristics. This advantage of easier control is overshadowed by emission levels which are far higher than those reported for contemporary, ultra-lean, dual-fuel RCCI concepts, where combustion is fully controlled by reaction kinetics (Paykani et al., 2016).

Thus, the goal of the present work is to develop a physics-based, RTM to predict the performance of cutting-edge RCCI marine engines. The methodology, although based on the work of Turesson et al. (Turesson, 2018), is adapted to this novel, low-emissions, combustion regime. Furthermore, the RTM is linearised based on a higher fidelity in-cylinder combustion model, i.e., a recently developed multizone model (Vasudev et al., 2022b). The whole modelling framework is validated against experimental data from a large-bore engine using dual-fuel (natural gas/diesel) LTC combustion with high mixture dilution rates. The RTM functionality is validated in several model-in-loop (MIL) case studies representing typical load transients and air-path disturbance rejection tests.

The final column of Table 1 highlights the key merits of the present work, in the context of advancing state-of-the-art LTC control orientated modelling. As such, the present RTM approach evidently inherits the advantages of both linear and physics-based models: fast in-cycle simulation time (5 ms), covering a wide speed range (both steady state and transient), and the merit of providing not only cycle-averaged combustion indicators, but also crank angle resolved cylinder pressure and heat release trends. Additionally, the resulting high estimation accuracy proves the modelling success. Within the scope of the current article, as indicated by the colours, the RTM is limited to combustion prediction, with fuel value and BR as the control variables. The emission estimation and air-path control are not included at this current stage. Furthermore, this model has not yet been applied to model predictive control (MPC), hence yellow and red cells are used here to indicate the improvement potential.

The paper is organised as follows: Section 2.1 describes the experimental test engine configuration and Section 2.2 explains the detailed mechanism of the fully predicting RCCI plant model. Section 2.3 addresses the linear RTM development formulations and testing matrix. Finally, Section 3 exhibits the full diary of RTM calibration and validation results. The paper is further expanded with a thorough discussion and conclusion to clarify the work contribution and potential further application.

2. The object and methods

The present work proposes a method to derive a new RTM intended for closed-loop RCCI combustion control in marine engines. Fig. 2 isa schematic depiction of the model development workflow, showing several distinct phases. Phases 1 and 2 involved the development of a physics-based model capable of fully predicting RCCI combustion simulation and intended for fast - but not real-time - pre-calibration/optimisation studies. The first version of this model, referred to here as the UVATZ model has been presented in Vasudev et al. (2022a), along with detailed calibration considerations. The key points of this process are outlined below and are essential from the perspective of reproductivity of the results. To this end, Section 2.1 introduces relevant data of the engine test bed, plus a brief discussion of data production for model calibration and validation. The governing assumptions of the

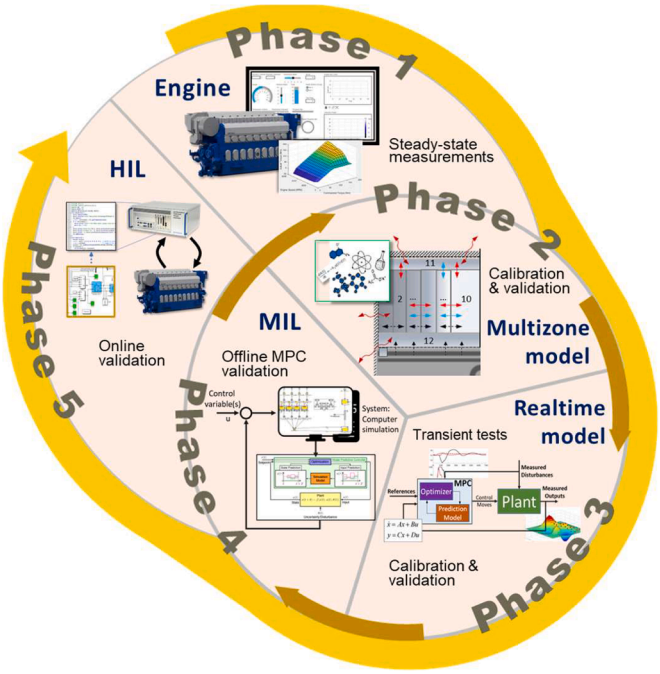

Fig. 2. Schematic of the model-based development workflow applied in this work.

UVATZ model are presented in Section 2.2, along with a brief summary of its validity.

Phase 3 in Fig. 2 is central to the present work. It covers the development and calibration of a linear physics-based RTM, followed by its validation against the UVATZ model. The UVATZ model is the basis for building the RTM by direct linearisation and also provides reference data for its extensive validation. Section 2.3 discusses linearisation, its detailed assumptions and underlying mathematical formalism. Section 2.4 gives a detailed account of the training and validation matrices. Phase 3s outcomes of RTM validation are discussed in the Results (Section 3), followed by an outlook toward phases 4 and 5 in the Conclusion (Section 4 and 5).

Note that the RCCI experiments from the single-cylinder research engine (SCRE) included only the steady- state characterisation of combustion in the governing operating points of the envelope. Thus, in Phase 2, the predictive feature of the UVATZ model was used to increase the density of the training data for virtual calibration of the RTM, including several transient scenarios, relevant for RCCI control. This model-based methodology can handle the system complexity/development time issues mentioned in the introduction.

2.1. The test object

The approach is validated using measurement data from a Wärtsilä SCRE operating in RCCI mode. It is derived from Wärtsiläs commercial W31DF marine engine category, a two-stage turbocharged, dual-fuel (DF) engine employing the lean-burn principle when operating with natural gas (NG) as the main fuel (Åstrand, Aatola, & Myllykoski, 2016). It has a multi-point gas injection system located upstream of the intake valve, and a twin-needle direct injector (Jay, D., 2016) for admission of the HRF.

Table 2 provides key specifications of the SCRE. For RCCI combustion, liquified natural gas (LNG) with methane number of 80 is used as the LRF; the HRF is light fuel oil (LFO), which is directly injected. The injector tip for LFO is changed to one with smaller nozzles that aid atomisation for low injection quantities. Additionally, the cone angle is narrower, to support HRF stratification during the early injection timing required for RCCI.

Table 2
Test engine setup.

Systems	Configuration
Displacement & nominal speed	32.45 l / 720 rpm
Stroke/bore	1.39
Air system	External air compressor with air temperature and pressure control (up to 10 bar)
HRF system	ISO 8217-compliant LFO; common rail 2.0 with twin-needle injector; and multi-injection capability
LRF system	ISO 8217-compliant LNG(MN=80); low-pressure, multi-point, upstream of the intake valves
Valvetrain	Four valves; variable intake valve closure (VIC)
Emission system	Horiba Mexa-One (NO_X, CO, THC, CO_2, O_2) AVL415S (FSN-soot)
Indicative system	AVL Indicom, cylinder pressure transducer Kistler 6124A, 300 bar range, 30pC/bar sensitivity.
Control system	Speedgoat rapid control platform

The validation data is produced at each steady-state operating point, with crank-angle-based cylinder pressure data from 300 consecutive cycles with 0.2 crank-angle degree (CAD) resolution. The in-cylinder pressure is further post-processed to obtain high frequency combustion indicators, like IMEP, CAX, PRR, etc. Other relevant measurement and data include the consumption of individual fuels and receiver air, component temperatures and detailed thermal characterisation of the charge at intake and exhaust ports.

2.2. The UVATZ predictive thermo-kinetic model

A physics-based model developed by Vasudev et al. (2022a) was used to produce the large amount of data required for training the RTM. The approach aims to capture RCCI combustion within a quasi-dimensional, multi-zone framework. This thermo-kinetic model is capable of simulating the influence of IVC conditions, in-cylinder fuel blending, thermal stratification and turbulence-based mixing. It can also reproduce the full in-cylinder pressure trace and emissions. The simulation framework coarsely divides the in-cylinder volume into reacting pockets called zones, each of which is essentially a homogeneous reactor with its own thermodynamic state. The arrangement of zones captures the in-cylinder thermal and compositional stratification, as typically observed in LTC CFD simulations (Fig. 3), yet within a fraction of the computation time.

The zones are coupled together by the requirement of equalised pressure within the MZM at any instant of time. This assumption alleviates the need for a momentum conservation equation. Therefore, the interzonal boundaries are free to move, depending on the thermodynamic state of neighbouring zones, resulting in interzonal work exchange (black arrows in Fig. 3). To capture the bulk effects of fluid motion on combustion, heat ($\dot{Q}$) and mass ($\dot{m}$) flow occurs between zones depicted by the red and blue arrows respectively. The flows are modelled on thermal and composition gradient ($\Delta T/\Delta w$ and $\Delta Y_i/\Delta w$ respectively) and scaled by the factor ζ_t shown in Eq (1) and Eq (2), where A is the flow area, $\mathfrak{D}$ is the mass diffusion coefficient, Λ is the thermal conductivity, and Δw is the distance between neighbouring zones (z) and ($z+1$). In addition, the Unity Lewis assumption (Eguz, 2013) has been considered for the diffusion coefficients.

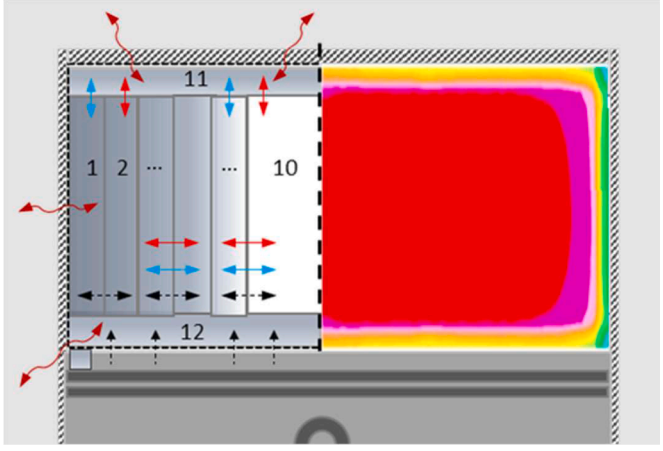

Fig. 3. Generalised MZ framework: red arrow – heat flow; blue arrow – mass flow; black arrow – work. MZM vs. CFD. (With permission from SAE).

$$^{IZT}\dot{m}_{i,z\to z+1} = \zeta_t \left(\mathfrak{D}\rho A \frac{\Delta Y_i}{\Delta w} \right)_{z\to z+1} \tag{1}$$

$$^{IZT}\dot{Q}_{z\to z+1} = \zeta_t \left(\Lambda A \frac{\Delta T}{\Delta w} \right)_{z\to z+1} \tag{2}$$

Wall heat loss is modelled according to the correlation by Chang et al. (2004), which is suitable for the temperature regime and convection-dominated heat transfer in LTC engines. For simulating NG-LFO RCCI combustion, NG is represented by n-alkanes up to C_2 and the surrogate for LFO is dodecane ($C_{12}H_{26}$). The mechanism by Yao et al. (2017) is chosen to describe the chemical kinetics of the fuel combination, and the justification is provided in Vasudev et al. (2022a). With NG premixed, diesel injection is simplified to the extent of mainly considering the vapour stratification before the onset of ignition. The profile is assumed linear in lambda domain and mapped onto the zones according to condition in Eq (3). λ_{global} is the in-cylinder air-fuel equivalence ratio of LFO; and R is the cylinder radius. ζ_λ is the λ_{LFO} in the outermost zone and is user-defined; and ζ_∇ is the slope of the profile which is calculated as satisfying the relation.

$$\lambda_{global} = \frac{1}{R}\int_0^R (\zeta_\nabla\, r + \zeta_\lambda) dr \tag{3}$$

At this development stage of the model, there are two tuning parameters: interzonal mixing intensity (ζ_t) and gradient of HRF stratification ζ_∇. These are associated with the interzonal flows and HRF stratification profile respectively and are case-dependent. The entire model is coded in C++ and uses Cantera (Goodwin et al., 2022) to handle the thermo-kinetic database. The inherently stiff system is solved using the CVODE solver (Hindmarsh et al., 2005). With the above-mentioned considerations, UVATZ requires 12 zones to capture the heat release profile within the target accuracy limits, while maintaining a simulation time of no more than 3 min/cycle on an Intel-Core i7 personal computer.

A more detailed explanation of the UVATZ model assumptions, including a broad analysis of its predictivity, can be found in another work by the authors (Vasudev et al., 2022a). In that study, the model was pre-calibrated to the current engine setup. Thus, for the purpose of the present work, the final validation of the model is discussed only briefly in the results section, and the reader is referred to the primary reference (Vasudev et al., 2022a) for greater detail.

2.3. The real-time model (RTM) for RCCI control

The approach of Turesson (Turesson, 2018) forms a basis for the construction of the RTM. This methodology was developed originally to control PPC applications. In essence, the approach uses heat release profile, including information on fuelling, to predict the following cycle's crank-angle-resolved in-cylinder pressure and heat release profile. This approach has been proven real-time capable (refer to Table 1), while maintaining a high degree of predictivity. The present works adopts this framework, but thoroughly reconsiders the submodel assumptions to make it applicable for phenomenologically more complex, dual-fuel RCCI combustion. The governing assumptions of the framework are:

- In transient operation, the change in heat release rate between consecutive combustion cycles is infinitely small compared to the difference in heat release between different engine operating points.
- Consequently, the heat release of the $k+1$ combustion cycle can be estimated from cycle k, by updating the change from cycle k.
- In-cylinder pressure at each CAD interval is reproduced from computed heat release using the first law of thermodynamics.
- In-cylinder temperature can be further obtained from equation of state, providing a baseline for semi-predictive modelling of thermal NOx.
- Consequently, the main modifications to the original approach, pertain to:
- Sensitivities of RCCI and PPC are different, resulting in a different choice of input parameters and correspondingly different linear submodels for these sensitivities.
- Due to the more volumetric nature of RCCI combustion, the control approach is based on cumulative heat release (CHR) instead of the heat release rate (HRR).
- The above method adds one computational step but is more robust, due to lower sensitivity to discretisation time step (avoiding aliasing at excessively heat release rates) and inherited filtering out reference signal disturbances.
- Start of combustion is modelled with reduced fidelity (map-based approach) to balance the simulation burden of the CHR method.

The above assumptions are discussed in more detail in the following subsections.

2.3.1. RTM input and output structure

Based on literature study(Koç & Şener, 2021; Taghavifar et al., 2021) and industrial practices (Storm et al., 2017; Wärtsilä, 2016), RCCI is sensitive to the intake conditions, with IVC, T_{int} and M_{egr} having the governing influences. For the current offline studies, the reference values for those parameters are taken from the detailed engine air-path model, built in GT-Suite. Note, however, that the rapid prototyping control module for further HIL tests already includes an isentropic valve flow submodel that enables estimation of those parameters in real-time, derived from the intake pressure measurement points, prior to initialising the heat release calculation. More on this real-time valve flow estimation method and its accuracy can be found in Valkjärvi et al. (2024). The current model application does not include variable valve actuation as a direct input for combustion control. Hence, the influence of these parameters is acknowledged in the model as disturbances D1 and D2 respectively. Fig. 4 depicts the general input-output structure of the RTM.

Fig. 4 shows that the primary outputs of the RTM are crank-angle-resolved CHR and in-cylinder pressure. All combustion indicators can be processed in real-time from these traces. The most important other indicators used in the results to discuss the validity of the approach are P_{max}, PRR, IMEP and CAX. The post-processing routine follows standard engine practice, and so is not discussed here. The RTM control inputs can be taken directly from the control unit and include the start of diesel injection and the corresponding injected fuel masses (m) of gas and diesel. From the perspective of future control implementation, these are fed to the model as total fuel energy (E_{fuel}) and energy-based gas-diesel BR. E_{fuel} and BR are defined in Eq. (4) and Eq. (5), respectively. Here $LHV\ (J/kg)$ denotes the lower heating values of diesel and gas, respectively.

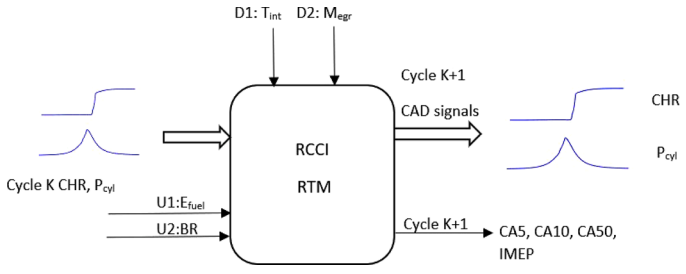

Fig. 4. RCCI real-time model input-output structure.

$$E_{fuel} = m_{gas} LHV_{gas} + m_{diesel}\, LHV_{diesel} \tag{4}$$

$$BR = \frac{m_{gas}\ LHV_{gas}}{E_{fuel}} \tag{5}$$

2.3.2. Mathematical framework of the RTM

The cycle-to-cycle RTM extends the method from Turesson, (2018) to RCCI, with the governing assumptions of small control input changes resulting in small CHR and cylinder pressure variations. One of the main improvements in the model compared to the original approach by Turesson et al. (2018) is the use of CHR instead of HRR, resulting in lower sensitivity to combustion aliasing. Overall, the applied methodology can be detailed as following steps:

- CHR estimation: the $k+1$ combustion cycle CHR is a sum of its cycle k measured CHR and the linear changes induced by the control actions.
- Combustion phase estimation: the calculated CHR curve is shifted along the crank-angle axis to represent the corresponding combustion phasing change. An earlier start of combustion (SOC) means a left shift; later SOC means a right shift.
- Cylinder pressure and IMEP estimation: the linear models from Turesson Turesson, 2018) are modified by adding tuneable parameters for RCCI control Eqs. (6) and ((7).

According to the cycle-to-cycle modelling principle (Henningsson, 2012; Turesson, 2018; Turesson et al., 2018), the next cycle's CHR, cylinder pressure (P_{cyl}) and IMEP are the sum of the previous cycle's CHR, P_{cyl} and IMEP, plus the induced changes in the corresponding model inputs U1 and U2 (E_{fuel}, and BR respectively). To this end, ΔU represents the cycle-wise change in the input. With the above assumptions, the system model can be expressed in linear form as in Eq. (6).

According to the framework assumptions, the previous cycle (cycle k) CHR is the initialisation of the RTM model. Its real-time calculation from directly measured in-cylinder pressure is already included in the engine control unit. The calculation methodology is standard first law analysis and so is not discussed in detail here. Readers interested in real-time heat release analysis are referred to the previous work by Storm et al. (2017). The effects of T_{int} and M_{egr} are also considered in Eq. (6). These parameters are influential yet cannot be imposed as direct control inputs. Hence, they are introduced as disturbance, incorporating additive unstructured uncertainty.

$$\begin{bmatrix} CHR(k+1) \\ P_{cyl}(k+1) \\ IMEP(k+1) \end{bmatrix} = \begin{bmatrix} CHR(k) \\ P_{cyl}(k) \\ IMEP(k) \end{bmatrix} + \begin{bmatrix} \frac{\partial CHR}{\partial E_{fuel}} & \frac{\partial CHR}{\partial BR} \\ \frac{\partial P_{cyl}}{\partial E_{fuel}} & \frac{\partial P_{cyl}}{\partial BR} \\ \frac{\partial IMEP}{\partial E_{fuel}} & \frac{\partial IMEP}{\partial BR} \end{bmatrix} \begin{bmatrix} \Delta E_{fuel}(k) \\ \Delta BR(k) \end{bmatrix} + \begin{bmatrix} D1_{chr}(k) & D2_{chr}(k) \\ D1_{P_{cyl}}(k) & D2_{P_{cyl}}(k) \\ D1_{imep}(k) & D2_{imep}(k) \end{bmatrix} \begin{bmatrix} T_{int} \\ M_{egr} \end{bmatrix} \tag{6}$$

The linear relation between the control inputs and CHR outputs is defined by Eq. (7), which indicates how a change in input is assumed to affect CHR, P_{cyl} and IMEP. To incorporate with the disturbance uncertainty for each output from T_{int} and M_{egr}, the zero-mean Gaussian process

random values of $D1_{chr}$, $D2_{chr}$, $D1_{pcyl}$ and $D2_{pcyl}$, $D1_{imep}$ and $D2_{imep}$ are introduced. The detailed values applied will be discussed in Section 3.3.

$$\frac{\partial CHR}{\partial E_{fuel}} = \frac{CHR}{E_{fuel}} \quad \frac{\partial CHR}{\partial BR} = \frac{a_1 \cdot CHR}{BR} \quad \frac{\partial \mathrm{P_{cyl}}}{\partial E_{fuel}} = \frac{d\mathrm{P_{cyl}}}{dE_{fuel}} \quad \frac{\partial \mathrm{P_{cyl}}}{\partial BR} = \frac{a_2 \cdot d\mathrm{P_{cyl}}}{dBR} \quad \frac{\partial IMEP}{\partial E_{fuel}} = \frac{dIMEP}{dE_{fuel}} \quad \frac{\partial IMEP}{\partial BR} = \frac{dIMEP}{dBR} \tag{7}$$

Note that Eq. (7) is inherited from work (Turesson, 2018), and modified in this work for RCCI. HRR and cylinder pressure $\mathrm{P_{cyl}}$ can be calculated from CHR, according to the first law of thermodynamics. The linearised pressure and IMEP are calculated according to the linear model from Turesson, (2018), the details are explained by the following equations.

The previous cycle HRR and CHR are measured and calculated according to the first law of thermodynamics:

$$\frac{dQ_c}{d\theta} = \frac{\gamma}{\gamma - 1} \frac{dV}{d\theta} P_{cyl} + \frac{1}{\gamma - 1} V \frac{dP_{cyl}}{d\theta} + \frac{dQ_{ht}}{d\theta} \tag{8}$$

$$Qc(\theta) = \int_{\theta_{IVC}}^{\theta} \frac{dQ_c}{d\theta} d\theta \tag{9}$$

Now one can relate a change in *u, Δu to a change in Qc, dQc/dϴ, dΔQc/dϴ.*

$$Qc(k+1) = Qc(k) + \frac{\partial\, Qc}{\partial E_{fuel}} \Delta E_{fuel}(k) + \frac{\partial Qc}{\partial BR}\ \Delta BR(k) \tag{10}$$

A change in E_{fuel} is assumed to affect the CHR:

$$\frac{\partial Qc}{\partial E_{fuel}} = \frac{Qc}{E_{fuel}} \tag{11}$$

A change in BR is assumed to affect the accumulated heat released:

$$\frac{\partial Qc}{\partial BR} = \frac{Qc}{BR} \tag{12}$$

The assumption of E_{fuel} influence on the CHR is straightforward. The same strategy is assumed here regarding the BR sensitivity impact. The overall CHR change due to changes in E_{fuel} and BR is assumed to be further equivalent to the effect of shifting *Qc* according to pre-calibrated maps. The predicted CHR is used to estimate the next cycle cylinder pressure, IMEP, CA10, CA50, and CA90.

From the estimated CHR and HRR, the next step is to predict how the pressure changes with the control inputs changes. Assuming weak cycle-to-cycle dynamics and small HRR shape variations when small changes in control inputs. Pressure model:

$$\frac{dP_{cyl}}{d\theta} = -\frac{\gamma}{V} \frac{dV}{d\theta} P_{cyl} + \frac{\gamma - 1}{V} \left(\frac{dQ_c}{d\theta} - h_c A \left(\frac{P_{cyl} V T_{IVC}}{P_{IVC} V_{IVC}} - T_w \right) \right) \tag{13}$$

With respect to P_{cyl} is the previous cycle pressure p^0, constant γ, and Tw. The linearised pressure is given by:

$$\frac{d\Delta P_{cyl}}{d\theta} = -\left(\frac{\gamma}{V} \frac{dV}{d\theta} + \frac{\partial \mu(P^0, \theta)}{\partial P_{cyl}} \right) \Delta P_{cyl} + \frac{\gamma - 1}{V} \frac{d\Delta Q_c}{d\theta} \tag{14}$$

The nonlinear term in the heat transfer is denoted:

$$\mu(P_{cyl}, \theta) = (\gamma - 1) \left(\frac{h_c A T_{IVC}}{P_{IVC} V_{IVC}} \right) P_{cyl} \tag{15}$$

ΔP_{cyl} can be computed from the solution to:

$$\Delta P_{cyl}(\theta) = \int_{\theta_{IVC}}^{\theta} \psi(\theta, \vartheta) \Gamma(\vartheta) \frac{d\Delta Q_c(\vartheta)}{d\vartheta} d\vartheta \tag{16}$$

$$\psi(\theta, \vartheta) = \exp\left(-\int_{\vartheta}^{\theta} \frac{d\mu\left(P_{cyl}{}^0, \tau\right)}{dP_{cyl}}\, d\tau \right) \left(\frac{V(\vartheta)}{V(\theta)} \right)^{\gamma} \tag{17}$$

$$\Gamma(\vartheta) = \frac{\gamma - 1}{V(\vartheta)} \tag{18}$$

The gradients with respect to P_{cyl} and IMEP can be calculated as

$$\frac{\partial \mathrm{P_{cyl}}}{\partial U} = \int_{\theta_{IVC}}^{\theta} \psi(\theta, \vartheta) \Gamma(\vartheta) \left(\nabla \frac{dQ_c(\vartheta)}{d\vartheta} \right) d\vartheta \tag{19}$$

$$\frac{\partial IMEP}{\partial U} = \frac{1}{V_d} \int_{V_{IVC}}^{V_{EVO}} \nabla P_{cyl} dV \tag{20}$$

In this way, the matrix B is calculated numerically, and this is updated every cycle based on the previous cycle's measurement data.

One needs to pay attention to the impact of Δ*BR* on CHR. In the above equation, $\frac{CHR}{BR}$ is always positive, while $\frac{\partial CHR}{\partial BR}$ could be positive or negative. This is why the coefficient a_1 from Eq. (7) is incorporated into the respective equation. Similarly, a_2 is assigned to determine the Δ*BR* impact on cylinder pressure changes. The values of a_1 and a_2 applied in this work for different cases are listed in Table 3.

As well as the explicit responses modelled by Eq. (7), each control input alters mixture reactivity, affecting combustion phasing. The framework assumption says that if the change in the control input is very small from cycle to cycle, the effect on combustion phasing can be reproduced by shifting the SOC while the overall shape of the CHR remains conserved (see Fig. 5). To this end, the difference in SOC for cycle $k+1$ compared to cycle k is denoted as ΔSOC and estimated using a rule-based map. The map is based on detailed UVATZ model responses, and the corresponding tuning parameters are explained in Tables 4 and 5. This simplified approach has proven to be as accurate as the physics-based SOC model used in the original work by Turesson et al. (2018), while cutting the RTM's simulation time by an order of magnitude. Note that the explicit results of the benchmark study for the RCCI-RTM, coupled with SOC submodels of different fidelity, have been presented by the authors in another study by (Modabberian et al., 2023).

Fig. 5 illustrates the methodology discussed above. As can be seen, from cycle k to $k+1$, when the E_{fuel} and *BR* increase, first, the initial CHR (blue line) is numerically increased correspondingly according to Eq. (7). The zoomed-in window of Fig. 5 shows that the entire CHR curve is right-shifted. The estimated RTM CHR (red line) is a good match trend-wise with the reference UVATZ CHR (green line). Marginal differences indicate a higher CHR peak and smaller ΔSOC from the RTM estimation.

To parameterise the above-mentioned coefficients a_1, a_2 and ΔSOC, a map is extracted according to the detail UVATZ model results. Implementation of the map uses a set of nested tables: Table 3 shows how the next cycle control responses are governed. The combustion phasing submodel is defined as a 1-D table with BR as the indexing axis and the corresponding absolute values of ΔSOC in crank-angle degrees (Table 4).

Table 3
RTM CHR calculation regulation map, with values based on the UVATZ calibration results discussed in Section 3.1.

ΔE_{fuel}	ΔBR	BR($k+1$)	a_1	a_2	ΔSOC [CAD]	Legend
0	0	–	+1	+1	0	0: no change
0	+	<=$\mathrm{br_{change}}$	+1	−1	- S	+: Increasing
		> $\mathrm{br_{change}}$	−1	−8	+S	S: 1-D map
+	0	–	+1	+1	- S	br_change: monotony
+	+	–	+1	+1	+1	transition point

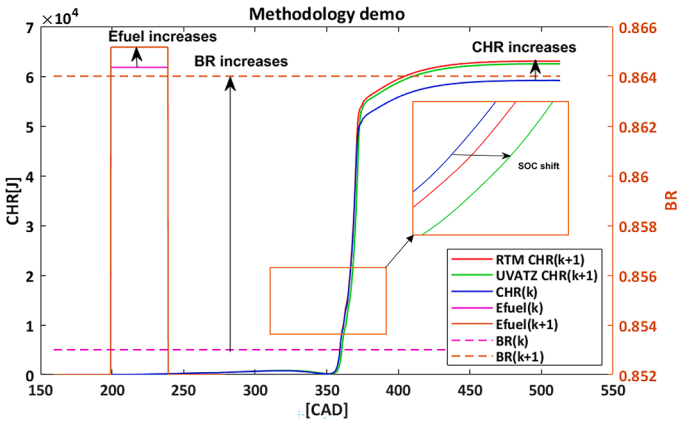

Fig. 5. RTM methodology demo with estimated next cycle CHR: when Efuel (left axis) and BR (right axis) are increasing, the next cycle CHR magnitude (left axis) will increase. The effect of input variables on combustion phasing is modelled by shifting the CHR curve along the crank-angle axis by a factor of ΔSOC (zoomed-in window).

2.4. The test matrix and model-based calibration/validation methodology

To calibrate and validate the proposed methodology, the RTM is compared with UVATZ simulations in both steady-state and quasi-transient conditions. The steady-state analysis focuses on two distinct RCCI operating points available from the Wärtsilä SCRE experimental campaign. The relevant model inputs for these two points, denoted as 1a and 1b, are set out in Table 5, referenced to the calibration of the commercial dual-fuel W31DF engine described in Section 2.1. With early SOI and elevated IVC temperature, the points represent purely kinetic-controlled RCCI combustion, phenomenologically compliant with the governing assumptions of the UVATZ model. At the same time, lower BR ensures that the fuel mixture is sufficiently reactive to enable a wide range of parametric analyses around the nominal conditions without encountering misfire limits.

The experimental results from these operating points were used for calibrating both RCCI models, UVATZ and RTM, at steady-state conditions. Due to the predictive nature of the UVATZ model, its results remain valid in the vicinity of the reference points. UVATZ is used to further generate data, outlined in cases 2 – 5 in Table 5. Parametric sweeps in cases 2a and 2b are used for calibrating the RTM. The calibration matrix for the RTM is thus deliberately limited to 20 points of cases 1 and 2, representing the variations of the primary model inputs, load and BR. This enables verifying the robustness of the RTM in terms of disturbance rejection (case 3) and in transient operation (cases 4 and 5). Note that the UVATZ model is used to provide reference results to validate the RTM in these scenarios.

3. Results

The results discussion aims to verify the assumptions of the RCCI RTM regarding accuracy, predictivity and robustness, as set out in Table 1. To this end, the discussion focuses on Phase 3 of the whole model-based development framework (see Fig. 2) and follows the case studies described above in Section 2.4.

3.1. RTM model calibration

The RTM model calibration involves tuning the coefficients for the *BR* and E_{fuel} response submodels as provided in Eq. (6). The nuances of tuning the SOC submodel (Table 4) are discussed below in Section 3.1.1. Calibration of the predictive UVATZ model, used here for virtual calibration of the RTM, has been comprehensively discussed in another study by Vasudev et al. (2022a). To maintain focus on the present work's key issue, the partial calibration results of the UVATZ model are omitted. Instead, Section 3.1.2 gives a brief account of UVATZ model validity, accompanied by validation results of the calibrated RTM

Table 4
The ΔSOC map nested in Table 3, with values based on the UVATZ calibration results discussed in Section 3.1.

BR	0.73	0.75	0.77	0.79	0.81	0.83	0.85	0.87	0.89	0.91	0.93
S (CAD)	0.2	0.2	0.6	1	1.2	1.6	1.8	2	2.2	3	3.8

Note that the br_{change} is obtained by analysing the UVATZ BR transient condition results. As indicated in Table 3, when only BR is increasing, br_{change} is defined as the boundary BR, where cylinder pressure amplitude changes rapidly, different a_1 and a_2 are applied. In this work, it is defined as an IMEP-based (8.6 bar–17.1 bar) linear interpolation of BR vector (0.75–0.89). Details will be discussed in Section 3.1.1.

Table 5
Scope of performed RCCI experiments with different toolchains, including steady-state real-engine tests and model-based transient simulations. Data values show variance from baseline reference of the standard IMO TIER III 25 % load calibration of the commercial variant of the W31DF, due to confidentiality constraints.

Campaign			Case #	$IMEP_g$ [bar]	BR [pp]	SOI [CAD]	T_{int} [K]	λ [−]	M_{egr} [%]	Number of RTM cases [−]
Experimental Calibration		Steady state	**1a**	9	ref	ref	ref	ref	4.84	1
					−11	−65	+20	+1.1		
			1b	16	ref	ref	ref	ref	5.35	1
					−2.5	−84.5	+7.5	−0.8		
Model-based study	Virtual RTM Calibration		**2a**	1a	$-7 \overset{1a}{\longleftrightarrow} +3$	1a	1a	1a	1a	10
			2b	1b	$-15 \overset{1b}{\longleftrightarrow} +3$	1b	1b	1b	1b	8
	Disturbance sensitivity	$\mathbf{T_{int}}$	**3a**	1a	1a	1a	$-3 \overset{1a}{\longleftrightarrow} +3$	1a	1a	12
		$\mathbf{M_{egr}}$	**3b**	1a	1a	1a	1a	1a	$-2 \overset{1a}{\longleftrightarrow} 2$	8
		$\mathbf{T_{int}}$ + $\mathbf{M_{egr}}$	**3c**	1a	1a	1a	$-3 \overset{1a}{\underset{random}{\longleftrightarrow}} +3$	1a	$-2 \overset{1a}{\underset{random}{\longleftrightarrow}} 2$	11
	Transient	λ	**4a**	$9 \leftrightarrow 16$	1a	1a	1a	$1a \leftrightarrow 1b$	1a	11
		Load	**4b**	$9 \leftrightarrow 16$	$1a \leftrightarrow 1b$	$1a \leftrightarrow 1b$	$1a \leftrightarrow 1b$	$1a \leftrightarrow 1b$	$1a \leftrightarrow 1b$	11
		Load + noise	**5**	$1a \leftrightarrow 1b$	$1a \leftrightarrow 1b$	$1a \leftrightarrow 1b$	$1a \overset{\pm 3}{\underset{random}{\longleftrightarrow}} 1b$	$1a \leftrightarrow 1b$	$1a \overset{\pm 0.5}{\underset{random}{\longleftrightarrow}} 1b$	11

model.

3.1.1. The primary response calibration

A sensitivity study of the parameters in Tables 3 and 4 was conducted to calibrate the RTM model. The findings were compared with the UVATZ model results. The calibration outcomes are shown in Table 5, cases 2a and 2b. Fig. 6 shows parameter a_2 sweep results with closed cycle in-cylinder pressure and P_{max} comparisons. It is evident in from Fig. 6 that the RTM and UVATZ model cylinder pressure results coincide appropriately with the experimental results. As expected from the calculation, the higher the a_2, the lower the P_{max}. Overall, the RTM model is able to capture the linear change trend of the P_{max}. The RMS error of each a_2 case is marked in a dashed line in Fig. 7, showing a maximum 5 bar error when compared with the UVATZ model result, and the nominal case with around 2 bar error.

In addition to the calibration of a_2, the applicable condition thereof is directly determined by the next cycle's BR. It is divided into two sections; smaller/equal and bigger than br_{change}. Based on the UVATZ BR transient result, br_{change} is defined as the operating point where cylinder pressure changes dramatically from the previous cycle as in Fig. 8a_2 is required to capture the fast P_{max} variation. For instance, in Fig. 8 the br_{change} of test case 2a is defined as 0.81 from where with the same 0.02 BR increasing, the peak pressure is decreased faster than lower BR cases.

In this work, br_{change} is defined as an IMEP-based (8.6 bar–17.1 bar) linear interpolation of the BR vector (0.75–0.89) and it is regarded as the nominal condition in Fig. 9. The br_{change} is crucial for identifying the transition point in the cylinder pressure model, sensitivity study of the br_{change} is demonstrated for case 2a in Fig. 9 by varying the br_{change} ±4 % from the nominal value. The 1st, 9th' and 10th cycles result in the same P_{max} error because of the distance from the br_{change} point. Cycles 2–5 have higher P_{max} errors when br_{change} decreases, and vice versa, cycles 7–8 have a higher error when br_{change} increases. This makes cycle 6, where BR is 0.81, the distinguishable point, from where higher BR requires a higher coefficient a_2. The P_{max} RMS error of 2 bars with nominal br_{change} setting from all cycles further proves the calibration result.

One also needs to pay attention to the IMEP calculation since it is based on cylinder pressure, and hence is affected by the coefficient a_2. To prove this, Fig. 10 illustrates the routine of adapting different $a_2$to IMEP calculation. As can be seen, the a_2 impact is overestimated when applying a_2 to IMEP calculation directly. Therefore, it can be concluded that a_2 should only be considered as a negative or positive sign. This

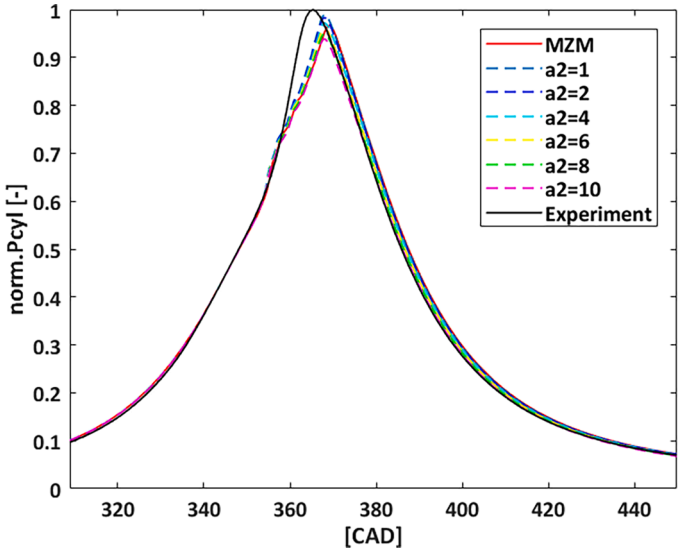

Fig. 6. Sensitivity study of the RTM tuning parameter a_2 impacts on cylinder pressure for test case 2a.

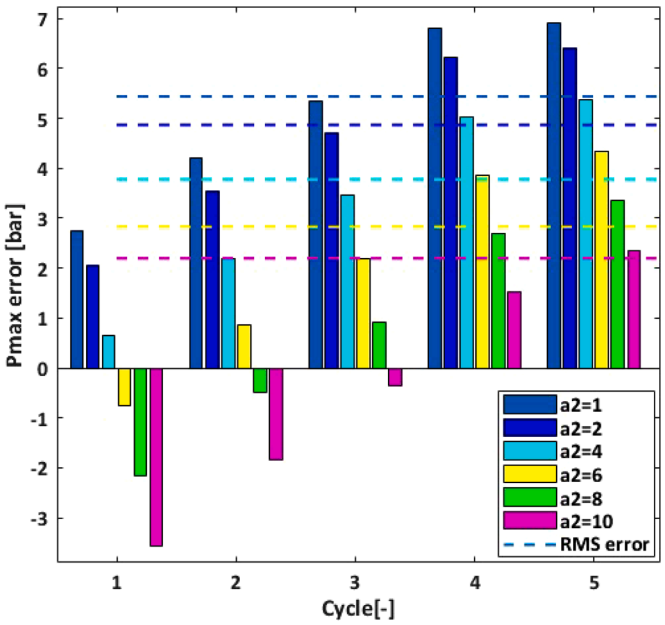

Fig. 7. Sensitivity study of the RTM tuning parameter a_2 impacts on P_{max} error for test case 2a. Dashed lines indicate the RMS errors of each case.

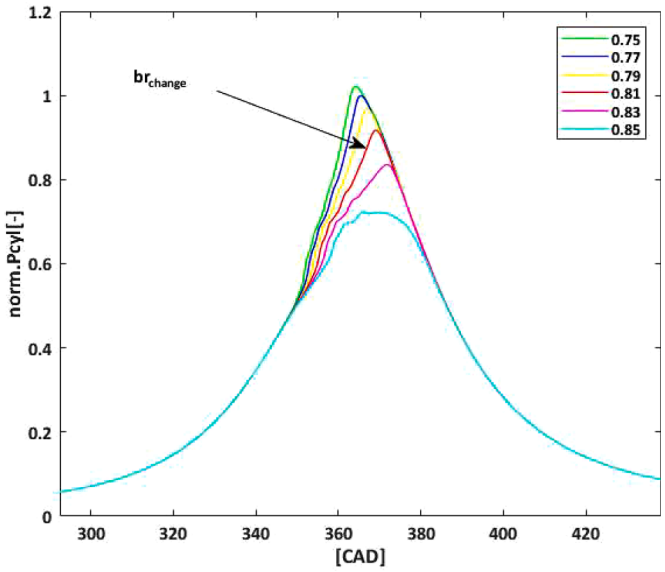

Fig. 8. br_change definition based on rapid change of cylinder pressure curve.

means, if $a_2$is assigned as −8, then the impact on IMEP must be −1, and vice versa: if a_2 is defined as 5, then the impact on IMEP shall be 1. This is illustrated in Fig. 10, where all positive a_2 values result in the same IMEP with a maximum error of ±0.1 bar. This stems from the fact that IMEP's impacts from control inputs are much smaller compared to cylinder pressure's. Therefore, implementation of the magnifier a_2 is not necessary for IMEP calculation.

The last tunable parameter from Tables 3 and 4 is the shifting parameter ΔSOC S. Thorough dissolution of the UVATZ simulation results provides the nominal S from Table 4. A sensitivity sweep of S in the span of nominal −0.2 and nominal +0.6 for case 2a promotes the calibration process. For brevity, Fig. 11 shows only the results of case 2a: the results of case 2b are qualitatively the same. As can be seen, there are clear linear CA5 and CA50 shifts along the CAD axis. In addition, the maximum RMS errors of CA50 and CA5 are around 0.7 and 1.2 CAD respectively, with the nominal case achieving RMS errors of 0.5 CAD for

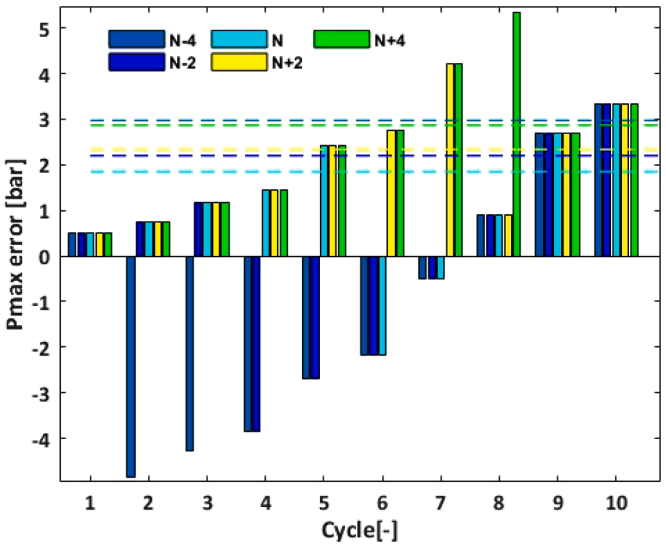

Fig. 9. br_{change} calibration result from test case 2a. RTM P_{max} error compared with UVATZ model where dashed lines are the RMS errors, and N denotes nominal value.

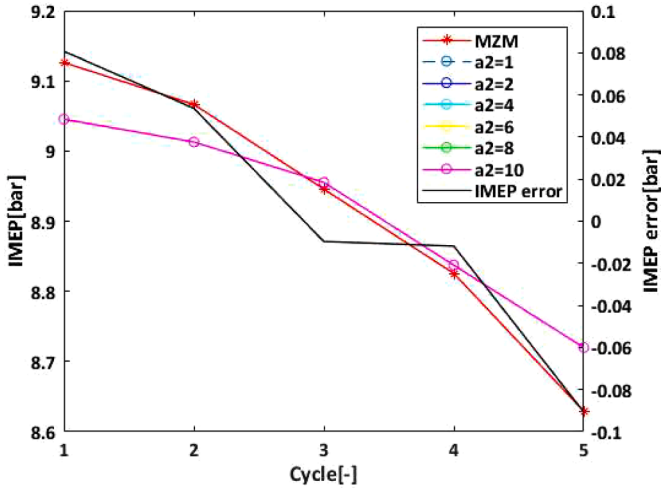

Fig. 10. Sensitivity study of the RTM tuning parameter a_2 impact on IMEP for test case 2a (invisible curves overlap each other). The black curve represents the IMEP error, with its y-axis on the right.

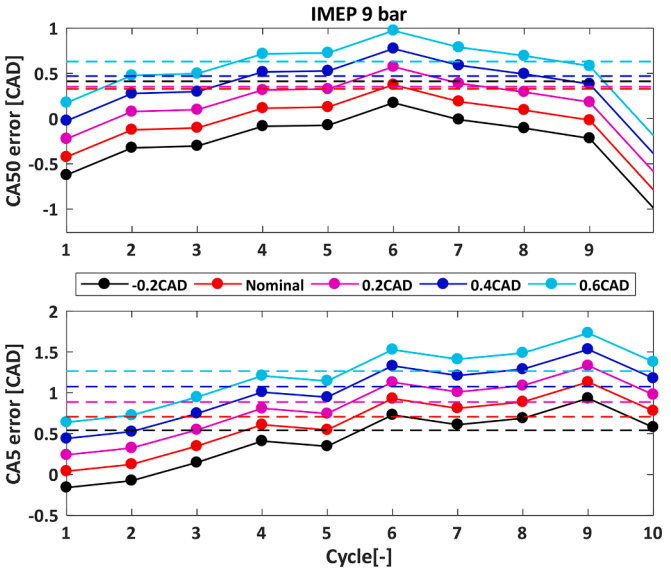

Fig. 11. Sensitivity study of the shifting impacts of RTM tuning parameter S on CA5 and CA50 for test case 2a. The dashed lines are the RMS errors of each cases.

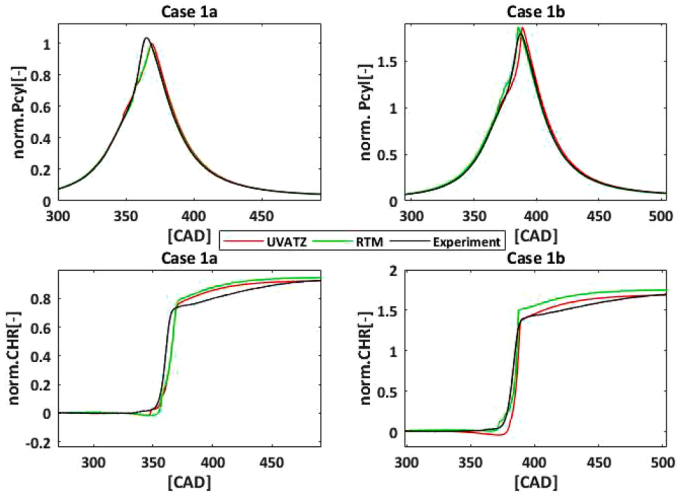

Fig. 12. UVATZ and RTM simulation results against experimental measurements of cylinder pressure and CHR for cases 1a and 1b.

CA50 and 0.6 CAD for CA5. In addition, considering the ultimate goal of combustion phase controller design, the CA50 accuracy result is prioritised to determine the S.

3.1.2. Accuracy targets for the RTM

The validation results of the UVATZ model and RTM were compared with the experimental measurements at two steady-state operating points which correspond to test cases 1a and 1b in Table 5. Fig. 12 depicts the comparisons of cylinder pressure and CHR traces. It is clear that the UVATZ model estimates the full cylinder pressure trend-wise with good accuracy. The main combustion indicator errors for both models are almost all below the defined error margin of 5 %, as indicated by Fig. 13. However, a slightly higher error is observed in CHR estimation of case 1b. The CHR traces from both UVATZ model and RTM show a slight mismatch compared with the experimental results, with RMS errors for CHR of 0.3 % and 3.5 % for UVATZ and RTM models respectively. Looking at the RTM model errors in Fig. 13, the only two estimation errors that are outside the defined 5 % margin are P_{max} and IMEP in case 1b, which exceed the margin by around 0.1 %. This inaccuracy arises because the RTM mainly has been tuned for low-load points, whereas case 1b is a high-load point. Furthermore, the BR in case 1b is very high, coming within in the boundary region where combustion starts to distort. The poorly tuned linear approximation is barely enough to capture this phenomenon, so the error is higher than in the low-load case.

To sum up, the sensitivity study explains the selection of tuneable parameters and demonstrates correct model behaviour with these parameters. The RTM's accuracy for the calibration cases falls very slightly short of the target set for the detailed UVATZ model, which is understandable due to reduced model fidelity. Bearing in mind the requirement for feed-forward combustion control (Hu et al., 2022), the accuracy target outside its calibration matrix for the RTM is ±7 % in all combustion indicators. The RTM is considered suitable for predictive model-based control if this accuracy criterion is satisfied for real-time simulation. The following sections verify this hypothesis.

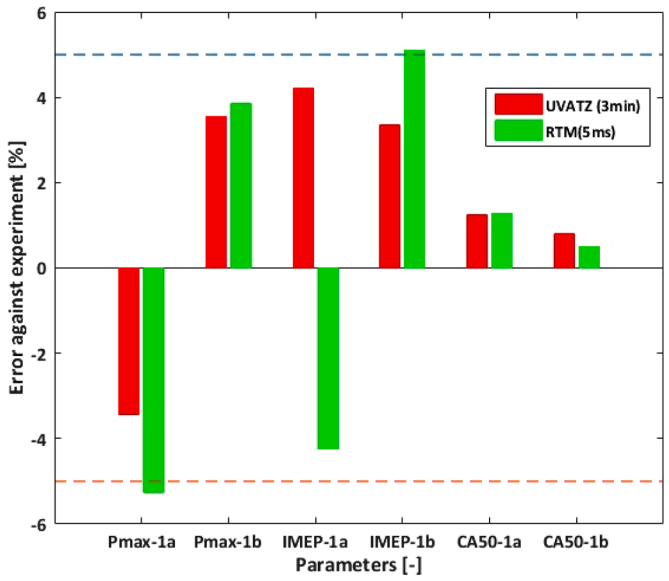

Fig. 13. UVATZ and RTM modelling errors against experimental results for combustion indicators for cases 1a and 1b: dashed lines indicate the target accuracy for the detail UVATZ model (±5 %).

3.2. RTM validation during transient condition

The validated UVATZ model has high predictivity (Vasudev et al., 2022a). This characteristic can be used to test and demonstrate the RTM's ability to cover transient conditions, which is missing from most MPC applications. The validation test covers transient operation where injected total fuel energy ΔE_{fuel} is varying in a span between mid-load point (IMEP 9 bar) to high-load point (IMEP 16 bar). There are constant and varying BR settings, as shown in Table 5, cases 4a and 4b. Case 4a is achieved by linearly varying the mass of fresh charge value from 1a to 1b, resulting in λ variation. Case 4b considers change in total fuel energy at a fixed BR. Thus, cases 4a and 4b assess treatment of ΔE_{fuel} in the framework (Section 2.3.2).

3.2.1. Transient load with constant BR

The transient load of IMEP 9 bar to 16 bar with a constant BR 0.83 was explored, and the results are presented in Figs. 14 and 15. Note that CHR and cylinder pressure are estimated with good accuracy. However, cylinder pressure cannot capture the crank-angle-based dramatic nonlinear change, but with only mismatching of amplitude, which is extremely low in this case. Fig. 15 shows the estimation error of CA50 is mostly within 1 CAD, with an RMS error of 0.94 CAD. Estimation of CA5 has an RMS error of 0.97 CAD. IMEP estimation error has a maximum of 0.1 bar. The estimation error of P_{max} has an RMS of 5.5 bar. It is evident that the first-cycle errors are much higher than other cycles'. This is because of the boundary operating region where, at a low-load point, high BR leads to near-misfire condition, and thus, is more challenging for the linear RTM to predict the change. However, this test supports the feasibility of this approach for estimating ΔE_{fuel} impacts at different load points. In general, the main combustion parameters are estimated with good accuracy, proving linear methodology works well when exploring within the working zone with only ΔE_{fuel} varying. This concludes RTM has high accuracy in cycle-based estimation of combustion parameters, although crank-angle-based information is more challenging to capture with this simple linear model.

3.2.2. Transient load with varying BR

In practice, when the load is changing, BR has a significant impact on combustion efficiency. Bearing this in mind, test case 4b considers varying BR at transient conditions from mid- to high-load. The overall

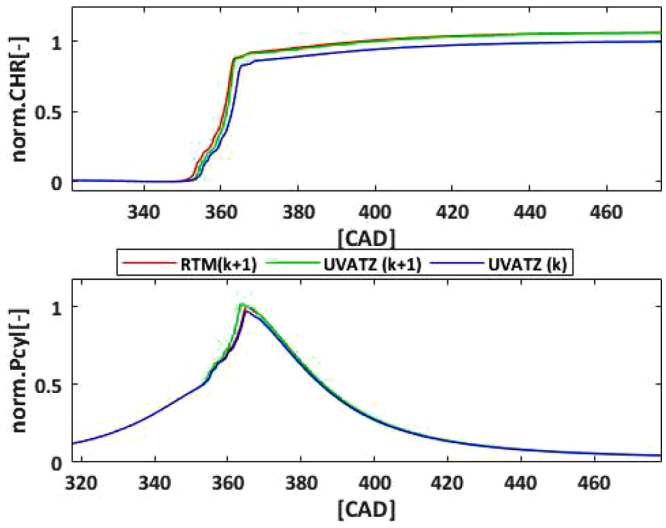

Fig. 14. RTM CHR and cylinder pressure estimation results compared with UVATZ model for test case 4a (IMEP 9–16 bar) load points with constant BR. The current cycle is indicated as k, next cycle is $k + 1$.

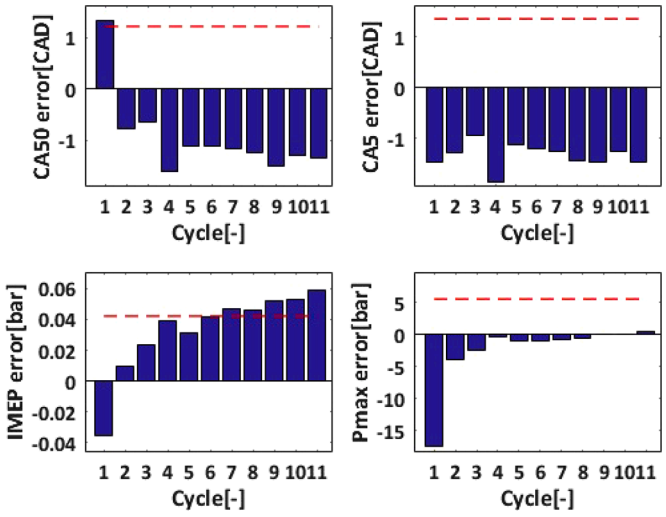

Fig. 15. RTM estimation error when compared with UVATZ model for test case 4a (IMEP 9–16 bar) with constant BR in all cycles, and the dashed lines are the RMS errors.

result is similar to test 4a, trend-wise, with high accuracy CHR and decent cylinder pressure, yet with demerit at momentarily crank-angle-based change, as seen in Fig. 16. An RMS error of 6.3 bar in P_{max} (Fig. 17) indicates overall reasonable accuracy. The pressure rise rate, (Fig. 16) has a maximum error of around 3 bar/CAD. However, this can vary significantly in each cycle because this method's simplicity prevents it from capturing the pressure change due to the nonlinear combustion phenomenon. This further demonstrates that the method of magnifying the cylinder pressure cannot capture accurately the nonlinear shifting and deformation. Nevertheless, this method allows P_{max} to be estimated within a narrow CAD window, which reduces the modelling complexity and computation time. A high pressure rise rate error is seen, especially in high-load conditions. This stems from the fact that there are dramatic changes in combustion efficiency at high-load conditions with dynamic input variations. However, the RTM model manages to achieve RMS errors of 0.84 CAD, 1.39 CAD and 0.08 bar for CA50, CA5, and IMEP respectively. It is evident in Fig. 17 that the errors resulting from cycles 10 and 11 are higher than those in other cycles. This is because high BR

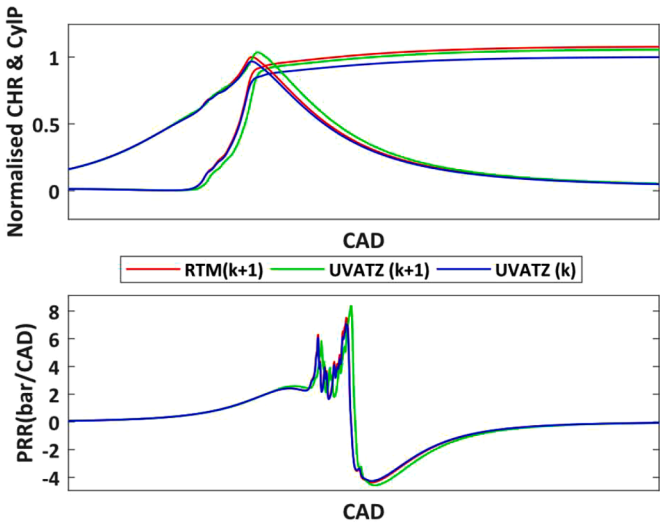

Fig. 16. CHR, cylinder pressure estimation result, and PRR error with different BR for test case 4b cycle 3.

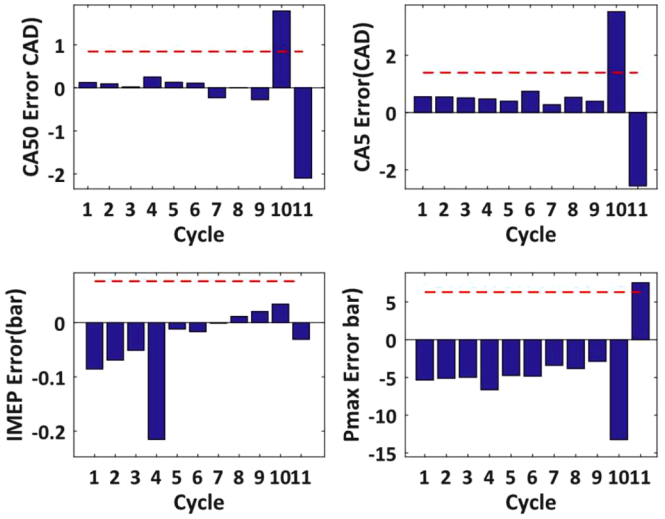

Fig. 17. RTM estimation error when compared with UVATZ model for test case 4b (IMEP 9–16 bar) with different BR.

pushes the combustion to the boundary region where combustion is changing extremely rapidly. On the other hand, this may bring a solution to use the pressure estimation error in control design to track the working region, so that fast control can be reacted to avoid entering the unstable zone.

The overall result indicates the predictability of the RTM model with trend-wise high accuracy in CHR and decent cylinder pressure, but with demerit at momentarily crank angle-based change. As already mentioned, pressure details cannot practically be captured accurately by a linear model. A more accurate cylinder pressure model would be needed for further development and higher accuracy. However, the main combustion parameters can be estimated with excellent accuracy for control design.

To further demonstrate the methodology's feasibility, the transient resolution was doubled. This entailed ramping-up from the same mid-load to high-load in only five cycles, by enlarging the ΔBR and ΔE_{fuel}. Fig. 18 presents the estimation error when compared with the UVATZ model result. First, it is clear to see that the last cycle's error is higher than that in the previous cycles. Once again, this is due to the linear model's failure to predict combustion with good precision where the BR

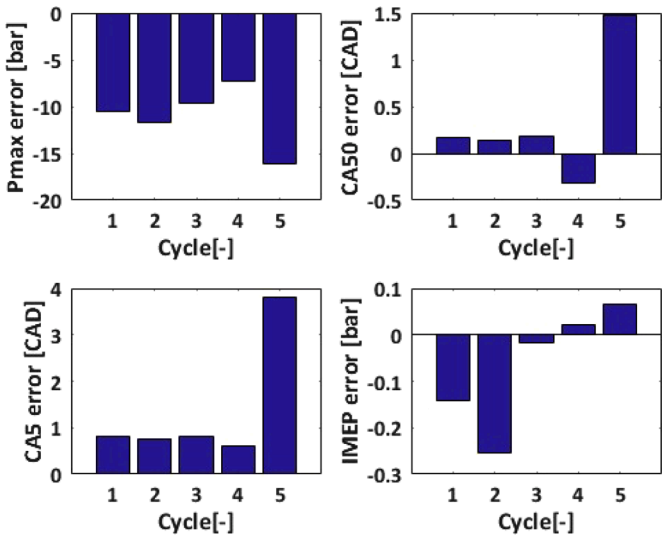

Fig. 18. P_{max}, CA50, CA5, and IMEP estimation error when ramping-up from mid-load to high-load in five cycles.

is near the high boundary condition. Second, when comparing Figs. 17 and 18, it is apparent that errors in all parameters are slightly higher when the control input changes are higher. However, the overall results still show good accuracy, with RMS errors of 0.12 bar for IMEP, 0.8 CAD for CA50, 1.8 CAD for CA5 and 11 bar for P_{max}. This reflects the fidelity of the RTM model by demonstrating that a relatively large change of control inputs will not reduce the accuracy significantly, although entering the boundary operating zone can result in a large error.

3.3. RTM sensitivity to disturbances

A fully working model should also consider disturbances and uncertainties in the system. Performance of a closed-loop controller is affected by how accurately the disturbance model represents actual disturbances. Dominantly controlled by fuel chemical kinetics, RCCI is highly sensitive to the variation of in-cylinder conditions. These include variations in temperature, pressure and composition of the intake charge; the amount of residual gas; the cooling effect of port fuel; fuel reactivity, etc. (Jia et al., 2015; Dong et al., 2016; Li et al., 2018). Although this work assumed weak cycle-to-cycle variances, this does not mean disturbances were ignored. Cases 3a–3c in Table 5 focus on RTM disturbance sensitivity to uncertainty and variation of T_{int} and M_{egr}. This is because RCCI operation typically exhibits high cycle-to-cycle variability, with combustion phasing highly sensitive to IVC conditions. The sources of this variation could be residual gas amount, the cooling effect of port fuel or the fuel mixture's reactivity [61–63], but in the present work, T_{int} and M_{egr} were chosen to reflect the influence of cyclic fluctuations on combustion performance. Based on literature and from experience, the magnitudes chosen for fluctuation of T_{int} and M_{egr} were ±3 K and ±40 % (1.3 g) respectively. Cases 3a and 3b in Table 5 linearly vary T_{int} and M_{egr} individually, within the previously specified range. Case 3c tests their combined influence, with the disturbance sourced as random noises within the range of ±3 K and ±40 %. The data are generated at nominal conditions of 1a. Validation entails adding randomly generated ±3k T_{int} and ±40 % M_{egr} noises to the UVATZ model.

The predefined disturbance was added to the inputs of the UVATZ model and the impacts on the combustion indicators (IMEP, P_{max}, CA5, and CA50, etc.) were analysed to evaluate the effect of uncertainty and variation. Then the zero-mean Gaussian process was introduced to cope with the T_{int}-induced uncertainty, with a standard deviation (STD) of 4 bar to incorporate the modelling uncertainty and noise for P_{max}. Likewise, white noise with STD of 0.82 CAD, 0.4 CAD, and 0.02 bar was

introduced to incorporate the modelling uncertainties for CA50, CA5 and IMEP respectively. Similarly, Gaussian noise with STD of 0.1 CAD for the CA50 compensation, 0.04 CAD for CA5, 0.5 bar for P_{max} and 0.003 bar for IMEP was considered to represent the uncertainty from the M_{egr} noise. Finally, with this Gaussian process integrated into the RTM, the RTM was validated against the UVATZ model at the same mid-load point.

Fig. 19 presents the errors when comparing the Gaussian-integrated RTM with the UVATZ result. As can be seen, the RMS errors of IMEP, CA5, and CA50 are extremely low, at 0.03 bar, 0.6 CAD and 1 CAD respectively. The error in P_{max} is higher, with a maximum of 9 bar, but its RMS error of less than 5 bar (around 4 %) can still be considered as high accuracy for control applications.

3.4. RTM full-scale test

Finally, for transient condition validation, case 5 in Table 5 considers load transient between nominal conditions 1a and 1b, on top of which disturbances in T_{int} and M_{egr} are included. Case 5 is obtained by linearly varying the associated parameters in discrete steps within the range, as specified in Table 5. The aim is to assess whether the RTM can perform within target accuracy of ±7 % throughout test cases 3–5. A successful outcome would support the main thesis of this work by demonstrating the predictive features of the approach, with real-time simulation capability and high estimation accuracy (±7 %).

Case 5 in Table 5 is this last full factorial test, at the transient mid-load to high-load condition with varying BR, and random T_{int} and M_{egr} noises. Fig. 20 depicts the cycle-wise results of UVATZ and RTM models. The RMS errors for P_{max}, CA5, CA50 and IMEP are 8.6 %, 0.3 %, 0.6 % and 0.6 % respectively. The added disturbances from T_{int} and M_{egr} increase the combustion uncertainty and result in prediction difficulty. The P_{max} result deserves particular attention. Here, the high error stems from the fact that the raw UVATZ cylinder pressure has stochastic fluctuations, so filtering the raw cylinder pressure may help to reduce this error. Fig. 21 summarises the overall estimation results from test case 5. IMEP, CA5, and CA50 achieve the goal of a 7 % error margin, while P_{max} is higher. This underscores the challenge of in-cylinder pressure estimation.

Obviously, modelling real-world systems could entail uncertainties. It would be the duty of the controller (to be designed) to appropriately address those mismatches and show robustness. Another way could be applying some of the learning-based control approaches, like (Jiang et al., 2022), to adaptively estimate the uncertainty or the appropriate regularisation.

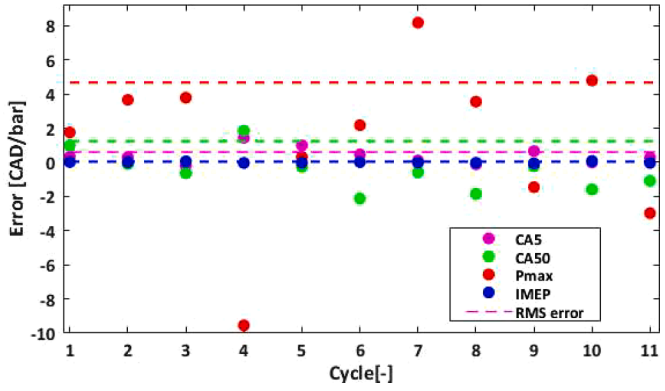

Fig. 19. Mid-load point CA5, CA50, IMEP, and P_{max} estimation error with proposed Gaussian disturbance models against the UVATZ model results. Dashed lines are the RMS error of each combustion indicator.

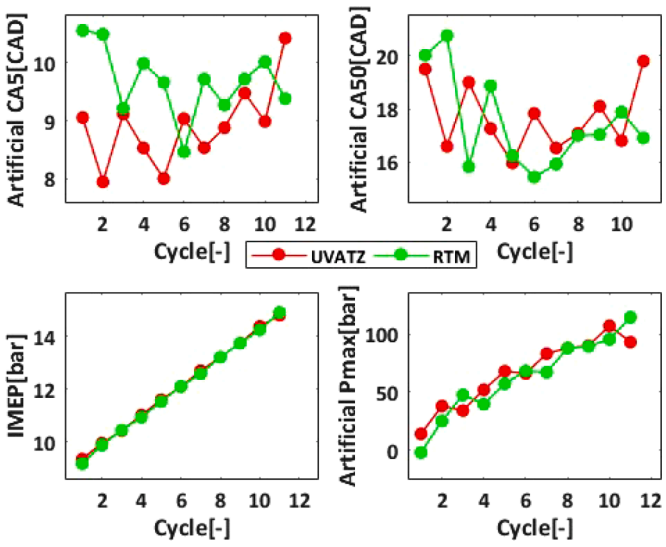

Fig. 20. Mid- to high-load CA5, CA50, IMEP, and P_{max} estimation result when compared with the UVATZ model result with added randomly generated T_{int} and M_{egr} disturbances.

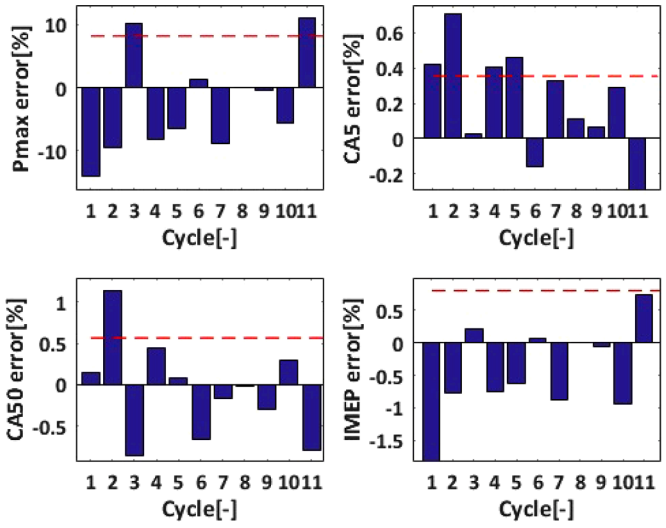

Fig. 21. Mid- to high-load CA5, CA50, IMEP, and P_{max} estimation error in% unit when compared with the UVATZ model result with added randomly generated T_{int} and M_{egr} disturbances. The dashed line indicates the RMS error in % unit.

4. Discussion and outlook

The results presented indicate that, within the order of significance, the RTM can reproduce the same trends in combustion indicators as the detailed physics-based RCCI combustion model, while being two orders of magnitude faster. The absolute-level accuracy was within the assumed 7 % error margin target for all quantities except P_{max}, for which momentary deviations were twice as large (up to 9 bar absolute difference). The uncertainty of the RTM in this respect requires a more focused analysis.

Closer inspection of the results regarding transient conditions and sensitivity to disturbances (Sections 3.2 and 3.3 respectively) prompts the hypothesis that the cause of the increased uncertainty of the P_{max} prediction is attributable to the detailed UVATZ model, rather than the RTM. This is illustrated in Fig. 22, which shows the results of the load sweep of Table 5's test case 4b from a different perspective. While linearly changing the fuel energy content, the primary responses should

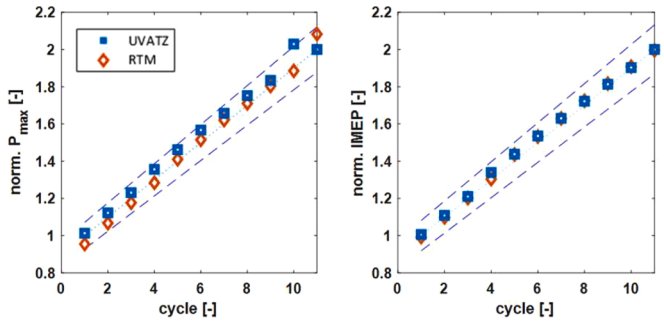

Fig. 22. Comparing results of P_{max} with IMEP between UVATZ and RTM for load sweep (test case 4b). Dashed line depicts 5 % deviation margin from linear trend (dotted) line. Data is normalised such that '1′ on y-axis represents operating conditions of case 1a and '2′ represents that of case 1b.

also be linear as soon as the RCCI combustion regime is maintained. This reasoning is the governing assumption of the RTM. However, while the IMEP predicted by both models follows this trend, the P_{max} values predicted by the UVATZ model show large-scale deviations from linearity. This is particularly visible in cycle number 4 and 10 in Fig. 22.

Note that the UVATZ model solves detailed chemical kinetics in a limited number of zones in order to maintain full predictivity within acceptable simulation times. Phenomenologically, these zones ignite with an order determined by fuel and thermal stratification in the cylinder. The UVATZ's HRR signal is thus a superposition of heat released through the combustion of individual zones, yielding a "spiky" signal that cannot be directly reconciled with real-world experimental results. When integrated, however, this gives a good representation of the experimental CHR and resulting combustion indicators, CA5 and CA50. On the other hand, the variations in the UVATZ HRR are directly transferred to the reproduced pressure signal, which becomes noisy. This can be seen in the PRR results in Fig. 16. Consequently, a very small change in individual species concentration in individual zones, caused by the large sensitivity of the involved detail kinetic mechanism, can lead to what may be percieved as stochastic changes to PRR and resulting bulk peak pressure. In other words, the kinetic nature of the UVATZ model trades-off superior predictivity with sensitivity to numerical stability issues. This occasionally manifests in over- or under-predicted P_{max} and PRR.

The above discussion substantiates the hypothesis that the reported uncertainty in P_{max} estimation is a consequence of this study's model-based calibration approach. We do not expect to see this issue when the RTM is re-validated against experimental data. Nevertheless, the currently reported 8.6 % error margin in P_{max} is already considered sufficient for control applications. The successful verification of the hypothesis raised above will pave the way to setting a tighter limit for the controller.

The next stages to be undertaken in the workflow depicted in Fig. 2 are design of the model-predictive controller for RCCI, based on the RTM (Phase 4); and the complete experimental validation of the model-based framework (Phase 5). In addition to these endeavours to demonstrate the feasibility of the developed toolchain for RCCI control, further incremental improvements of the RTM are envisaged. In this regard, the present work identifies two primary research areas. The first of these is extending the RTM predictivity by the inclusion of a physics-based ignition delay model. The initial results of this extension can be found in the work by Modabberian et al. (2023). The second research area is extension of the RTM functionality by including additional inputs and phenomenological emission submodels. This track is expected to take the model beyond the state of the art for LTC control approaches, as discussed in Table 1.

There also is potential for in-cycle control applications for the anticipated RTM developments. The current version of the RTM completes a single RCCI combustion cycle simulation within 5 ms, running on a personal computer (Intel i7–11850H@2.5 GHz processor) without code optimisation to include dedicated real-time solvers. For the mid-speed marine engine application considered here (four-stroke, 750 rpm), the real-time limit for a single combustion cycle is 160 ms ($2 \times 60/750 = 160$ ms).

Readers are referred to the Clean Propulsion Technologies Project website (*Clean Propulsion Technologies*, 2022) for the latest list of publications covering developments of the present work.

5. Conclusions

This paper describes development of a novel, physics-based cycle-to-cycle real-time combustion model (RTM) for cutting-edge, dual-fuel marine engines operating in reactivity-controlled compression ignition (RCCI) mode. The RTM's calibration is based on the steady-state results obtained from a single-cylinder research engine representing the next-generation Wärtsilä 31DF platform. Transient tests are extrapolated using a previously acclaimed, fully predictive thermo-kinetic combustion model referred to as UVATZ.

The work makes the following conclusions:

- Accurate real-time modelling of primary RCCI control responses (fuel energy and BR) is possible using the observation from a previous cycle's cumulative heat release. The primary model structure is physics-based (in-cylinder pressure, temperature estimation) while linearising the change in heat release and start of combustion.
- The developed RTM predicts all in-cylinder pressure-derived combustion indicators within a 7 % error margin target compared with steady-state experimental results.
- Transient tests verify that the RTM achieves satisfactory results in terms of combustion phasing and IMEP. The RMS errors in CA5 and CA50, compared to the detailed UVATZ model, are below 1.5 CAD. IMEP is predicted with absolute accuracy of 0.8 bar.
- Dedicated disturbance rejection tests confirm the RTM's ability to handle 10 % variations of in-cylinder charge temperature and internal EGR, while maintaining similar accuracy.
- Overall, the prediction accuracy during steady-state test conditions is better than in the transient case. The accuracy is strongly related to the combustion region; poorer accuracy is observed when approaching stable combustion boundary conditions, where misfire or knocking may occur.
- Peak in-cylinder pressure results show by far the highest RMS error in all test cases. The peak error of 8.6 % (up to 12 bar absolute differences) seems attributable to the numerical sensitivity of the detailed thermo-kinetic model reference. The RTM is expected to perform well within the 7 % error margin target if high-quality experimental data are used as a reference.

The above results demonstrate that the proposed RTM offers unprecedented predictivity compared to previous, more-simplistic RCCI combustion models. The RTM also overcomes the complexity versus simulation time dilemma. With simulation times below 5 ms per RCCI combustion cycle, the RTM is considered suitable for model-predictive RCCI combustion control. Furthermore, a large real-time surplus allows extending the present approach towards real-time emission modelling.

Declaration of Competing Interest

The authors declare that they have no known competing financial interests or personal relationships that could have appeared to influence the work reported in this paper.

Acknowledgments

The work was conducted in the framework of the Clean Propulsion

Technologies project with financial support from Business Finland (ref. 38475/31/2020).

Supplementary materials

Supplementary material associated with this article can be found, in the online version, at doi:10.1016/j.conengprac.2023.105724.

References

Modabberian, A., Storm, X., Vasudev, A., Zenger, K., Hyvönen, J., & Mikulski, M. (2023). Towards real-time combustion phase estimation for linear RCCI model-predictive control design. In *IFAC World Congress 2023*.

Agarwal, A. K., Singh, A. P., & Maurya, R. K. (2017). Evolution, challenges and path forward for low temperature combustion engines. *Progress in Energy and Combustion Science, 61*, 1–56. https://doi.org/10.1016/j.pecs.2017.02.001

Ahmad, Z., Kaario, O., Qiang, C., Vuorinen, V., & Larmi, M. (2019). A parametric investigation of diesel/methane dual-fuel combustion progression/stages in a heavy-duty optical engine. *Applied Energy, 251*, Article 113191. https://doi.org/10.1016/j.apenergy.2019.04.187

Albin Rajasingham, T. (2021). Introduction. *Nonlinear model predictive control of combustion engines* (pp. 1–16). Springer International Publishing. https://doi.org/10.1007/978-3-030-68010-7_1

Åstrand, U., Aatola, H., and Myllykoski, J. (2016). *Wärtsilä 31-world's most efficient fourstroke engine*.

Atkinson, C. (2014). *SAE Technical Paper 2014-01-2359*. SAE 2014 Commercial Vehicle Engineering Congress. https://doi.org/10.4271/2014-01-2359

Basina, L. N. A., Irdmousa, B. K., Velni, J. M., Borhan, H., Naber, J. D., & Shahbakhti, M. (2020). Data-driven modeling and predictive control of maximum pressure rise rate in RCCI engines. In *2020 IEEE Conference on Control Technology and Applications (CCTA)* (pp. 94–99). https://doi.org/10.1109/CCTA41146.2020.9206358

Benajes, J., Pastor, J. V., García, A., & Monsalve-Serrano, J. (2015). The potential of RCCI concept to meet EURO VI NOx limitation and ultra-low soot emissions in a heavy-duty engine over the whole engine map. *Fuel, 159*, 952–961. https://doi.org/10.1016/j.fuel.2015.07.064

Chang, J., Güralp, O., Filipi, Z., Assanis, D., Kuo, T.-W., Najt, P., & Rask, R. (2004). New heat transfer correlation for an HCCI engine derived from measurements of instantaneous surface heat flux. *SAE Transactions, Section 3: Journal of Engines, 113*, 1576–1593.

Clean Propulsion Technologies. (2022). https://cleanpropulsion.org/.

Dahodwala, M., Joshi, S., Koehler, E., Franke, M., & Tomazic, D. (2015). *SAE Technical Paper 2015-01-0849*. SAE 2015 World Congress & Exhibition. https://doi.org/10.4271/2015-01-0849

D.G. Goodwin, H.K. Moffat, Ingmar Schoegl, R.L. Speth, & B.W. Weber. (2022). *Cantera: An object-oriented software toolkit for chemical kinetics, thermodynamics, and transport processes*. doi:10.5281/zenodo.6387882.

Dempsey, A. B., Walker, N. R., Gingrich, E., & Reitz, R. D. (2014). Comparison of low temperature combustion strategies for advanced compression ignition engines with a focus on controllability. *Combustion Science and Technology, 186*(2), 210–241. https://doi.org/10.1080/00102202.2013.858137

Dong, S., Cheng, X., Ou, B., Liu, T., & Wang, Z. (2016). Experimental and numerical investigations on the cyclic variability of an ethanol/diesel dual-fuel engine. *Fuel, 186*, 665–673. https://doi.org/10.1016/j.fuel.2016.09.027

Dong, T., Liu, B., Zhang, F., Wang, Y., Wang, B., & Liu, P. (2017). Control oriented modeling and analysis of gas exchange and combustion processes for LTC diesel engine. *Applied Thermal Engineering, 110*, 1305–1314. https://doi.org/10.1016/j.applthermaleng.2016.09.001

Ebrahimi, K. (n.d.). *Model Based Control of Combustion Timing and Load in HCCI Engines*. 282.

Ebrahimi, K., Aliramezani, M., & Koch, C. R. (2016). An HCCI control oriented model that includes combustion efficiency. *IFAC-PapersOnLine, 49*(11), 327–332. https://doi.org/10.1016/j.ifacol.2016.08.049

Ebrahimi, K., & Koch, C. (2015). Model predictive control for combustion timing and load control in HCCI engines. In *SAE Technical Paper 2015-01-0822*. SAE 2015 World Congress & Exhibition. https://doi.org/10.4271/2015-01-0822.

Ebrahimi, K., & Koch, C. R. B. (2018). Real-time control of HCCI engine using model predictive control. In *2018 Annual American Control Conference (ACC)* (pp. 1622–1628). https://doi.org/10.23919/ACC.2018.8431211

García Valladolid, P., Tunestål, P., Monsalve-Serrano, J., García, A., & Hyvönen, J. (2017). Impact of diesel pilot distribution on the ignition process of a dual fuel medium speed marine engine. *Energy Conversion and Management, 149*, 192–205. https://doi.org/10.1016/j.enconman.2017.07.023

Guardiola, C., Pla, B., Bares, P., & Barbier, A. (2018). A combustion phasing control-oriented model applied to an RCCI engine. *IFAC-PapersOnLine, 51*(31), 119–124. https://doi.org/10.1016/j.ifacol.2018.10.022

Hanson, R., Ickes, A., & Wallner, T. (2016). *SAE Technical Paper 2016-01-0794*. SAE 2016 World Congress and Exhibition. https://doi.org/10.4271/2016-01-0794

Henningsson, M. (2012). *[Doctoral Thesis]*. Department of Automatic Control, Lund Institute of Technology, Lund University.

Hindmarsh, A. C., Brown, P. N., Grant, K. E., Lee, S. L., Serban, R., Shumaker, D. E., & Woodward, C. S. (2005). SUNDIALS: Suite of nonlinear and differential/algebraic equation solvers. *ACM Transactions on Mathematical Software, 31*(3), 363–396. https://doi.org/10.1145/1089014.1089020

Hu, J., Chen, Z., Yao, Y., Shi, L., & Deng, K. (2022). Study on control-oriented emission predictions of PPCI diesel engine with two-stage fuel injection. *Fuel, 320*, Article 123984. https://doi.org/10.1016/j.fuel.2022.123984

Indrajuana, A., Bekdemir, C., Feru, E., & Willems, F. (2018). *SAE Technical Paper 2018-01-0263*. WCX World Congress Experience. https://doi.org/10.4271/2018-01-0263

Irdmousa, B. K., Rizvi, S. Z., Veini, J. M., Nabert, J. D., & Shahbakhti, M. (2019). Data-driven modeling and predictive control of combustion phasing for RCCI engines. In *2019 American Control Conference (ACC)* (pp. 1617–1622). https://doi.org/10.23919/ACC.2019.8815269

Valkjärvi, P., Hissa, M., Kim, J., Storm, X., Söderäng, E., Mikulski, M., Chojnowski,J. , Szamrej, G. (2024). State-of-the-art in LTC review of engine measurement and data analysis. SAE International Journal of Engines (Unpublished manuscript).

Eguz, U. (2013). *Crossing the combustion modes in diesel engines* [Phd Thesis, Technische Universiteit Eindhoven]. doi: 10.6100/IR756736.

Jay, D. (2016). *CR development in the last decade in Wärtsilä*.

Jeyamoorthy, A., Degawa, T., Sok, R., Akimichi, T., Kurita, S., Ogawa, M., Takei, T., Hayashi, I., Kusaka, J., Zhou, B., Yamaguchi, K., & Tanabe, I. (2022). Development and comparison of virtual sensors constructed using AI techniques to estimate the performances of IC engines. In *SAE Technical Paper 2022-01-1064. SAE Powertrains, Fuels & Lubricants Conference & Exhibition*. https://doi.org/10.4271/2022-01-1064

Jia, M., Dempsey, A. B., Wang, H., Li, Y., & Reitz, R. D. (2015). Numerical simulation of cyclic variability in reactivity-controlled compression ignition combustion with a focus on the initial temperature at intake valve closing. *International Journal of Engine Research, 16*(3), 441–460. https://doi.org/10.1177/1468087414552088

Jia, Z., & Denbratt, I. (2015). Experimental investigation of natural gas-diesel dual-fuel RCCI in a heavy-duty engine. *SAE International Journal of Engines, 8*(2), 797–807. https://doi.org/10.4271/2015-01-0838

Jiang, Y., Gao, W., Na, J., Zhang, D., Hämäläinen, T. T., Stojanovic, V., & Lewis, F. L. (2022). Value iteration and adaptive optimal output regulation with assured convergence rate. *Control Engineering Practice, 121*, Article 105042. https://doi.org/10.1016/j.conengprac.2021.105042

Kahila, H., Wehrfritz, A., Kaario, O., & Vuorinen, V. (2019). Large-eddy simulation of dual-fuel ignition: Diesel spray injection into a lean methane-air mixture. *Combustion and Flame, 199*, 131–151. https://doi.org/10.1016/j.combustflame.2018.10.014

Kakati, D., Roy, S., & Banerjee, R. (2019). Development of an artificial neural network based virtual sensing platform for the simultaneous prediction of emission-performance-stability parameters of a diesel engine operating in dual fuel mode with port injected methanol. *Energy Conversion and Management, 184*, 488–509. https://doi.org/10.1016/j.enconman.2019.01.087

Kakoee, A., Bakhshan, Y., Barbier, A., Bares, P., & Guardiola, C. (2020). Modeling combustion timing in an RCCI engine by means of a control oriented model. *Control Engineering Practice, 97*, Article 104321. https://doi.org/10.1016/j.conengprac.2020.104321

Khodadadi Sadabadi, K., & Shahbakhti, M. (2016). Dynamic modelling and controller design of combustion phasing for an RCCI engine. ASME 2016 *Dynamic Systems and Control Conference, 2*. https://doi.org/10.1115/DSCC2016-9696.

Koç, M. A., & Şener, R. (2021). Prediction of emission and performance characteristics of reactivity-controlled compression ignition engine with the intelligent software based on adaptive neural-fuzzy and neural-network. *Journal of Cleaner Production, 318*, Article 128642. https://doi.org/10.1016/j.jclepro.2021.128642

Li, Y., Jia, M., Chang, Y., Xu, Z., Xu, G., Liu, H., & Wang, T. (2018). Principle of determining the optimal operating parameters based on fuel properties and initial conditions for RCCI engines. *Fuel, 216*, 284–295. https://doi.org/10.1016/j.fuel.2017.12.010

Mikulski, M., Balakrishnan, P. R., Doosje, E., & Bekdemir, C. (2018). *SAE Technical Paper 2018-01-0254*. WCX World Congress Experience. https://doi.org/10.4271/2018-01-0254

Mikulski, M., Balakrishnan, P. R., & Hunicz, J. (2019a). Natural gas-diesel reactivity controlled compression ignition with negative valve overlap and in-cylinder fuel reforming. *Applied Energy, 254*, Article 113638. https://doi.org/10.1016/j.apenergy.2019.113638

Mikulski, M., Bekdemir, C., & Willems, F. P. T. (2016). Experimental validation of a combustion kinetics based multi-zone model for natural gas-diesel RCCI engines (Trans.). In C. S. Technology, G. Somers, & E. H. T. Systems (Eds.), *2016 Symposium for Combustion Control (SCC 2016)* https://research.tue.nl/nl/publications/aa7ae4c5-3efa-4e3f-ad53-899e0ef7313b.

Mikulski, M., Ramesh, S., & Bekdemir, C. (2019b). Reactivity Controlled Compression Ignition for clean and efficient ship propulsion. *Energy, 182*, 1173–1192. https://doi.org/10.1016/j.energy.2019.06.091

Mikulski, M., Wierzbicki, S., & Piętak, A. (2015a). Numerical studies on controlling gaseous fuel combustion by managing the combustion process of diesel pilot dose in a dual-fuel engine. *Chemical and Process Engineering, 36*(2), 225–238. https://doi.org/10.1515/cpe-2015-0015

Mikulski, M., Wierzbicki, S., & Pietak, A. (2015b). Zero-dimensional 2-phase combustion model in a dual-fuel compression ignition engine fed with gaseous fuel and a divided diesel fuel charge. *Eksploatacja i Niezawodnosc - Maintenance and Reliability, 17*(1), 42–48. https://doi.org/10.17531/ein.2015.1.6

Molina, S., García, A., Pastor, J. M., Belarte, E., & Balloul, I. (2015). Operating range extension of RCCI combustion concept from low to full load in a heavy-duty engine. *Applied Energy, 143*, 211–227. https://doi.org/10.1016/j.apenergy.2015.01.035

Norouzi, A., Ebrahimi, K., & Koch, C. R. (2019). Integral discrete-time sliding mode control of homogeneous charge compression ignition (HCCI) engine load and combustion timing. *IFAC-PapersOnLine, 52*(5), 153–158. https://doi.org/10.1016/j.ifacol.2019.09.025

Paykani, A., Garcia, A., Shahbakhti, M., Rahnama, P., & Reitz, R. D. (2021). Reactivity controlled compression ignition engine: Pathways towards commercial viability.

Applied Energy, 282, Article 116174. https://doi.org/10.1016/j.apenergy.2020.116174

Paykani, A., Kakaee, A.-H., Rahnama, P., & Reitz, R. D. (2016). Progress and recent trends in reactivity-controlled compression ignition engines. *International Journal of Engine Research, 17*(5), 481–524. https://doi.org/10.1177/1468087415593013

Raut, A., Irdmousa, B. K., & Shahbakhti, M. (2018). Dynamic modeling and model predictive control of an RCCI engine. *Control Engineering Practice, 81*, 129–144. https://doi.org/10.1016/j.conengprac.2018.09.004

Reitz, R. D., & Duraisamy, G. (2015). Review of high efficiency and clean reactivity controlled compression ignition (RCCI) combustion in internal combustion engines. *Progress in Energy and Combustion Science, 46*, 12–71. https://doi.org/10.1016/j.pecs.2014.05.003

Scocozza, G. F., Silvagni, G., Brusa, A., Cavina, N., Ponti, F., Ravaglioli, V., De Cesare, M., Panciroli, M., & Benedetti, C. (2021). Development and validation of a virtual sensor for estimating the maximum in-cylinder pressure of SI and GCI engines. In *SAE Technical Paper 2021-24-0026. 15th International Conference on Engines & Vehicles*. https://doi.org/10.4271/2021-24-0026

Stanglmaier, R. H., & Roberts, C. E. (1999). *SAE Technical Paper 1999-01-3682*. International Fuels & Lubricants Meeting & Exposition. https://doi.org/10.4271/1999-01-3682

Storm, X., Salminen, H., Virrankoski, R., Niemi, S., & Hyvonen, J. (2017). *SAE Technical Paper 2017-01-1067*. WCX^{TM} 17: SAE World Congress Experience. https://doi.org/10.4271/2017-01-1067

Sui, W., Hall, C. M., & Kapadia, G. (2020). Cylinder-specific model-based control of combustion phasing for multiple-cylinder diesel engines operating with high dilution and boost levels. *International Journal of Engine Research, 21*(7), 1231–1250. https://doi.org/10.1177/1468087418804087

Taghavifar, H., Nemati, A., Salvador, F. J., & De la Morena, J. (2021). 1D energy, exergy, and performance assessment of turbocharged diesel/hydrogen RCCI engine at different levels of diesel, hydrogen, compressor pressure ratio, and combustion duration. *International Journal of Hydrogen Energy, 46*(42), 22180–22194. https://doi.org/10.1016/j.ijhydene.2021.04.035

Turesson, G. (2018). *Doctoral Thesis*. Department of Automatic Control, Lund Institute of Technology, Lund University.

Turesson, G., Yin, L., Johansson, R., & Tunestål, P. (2018). Predictive pressure control with multiple injections. *IFAC-PapersOnLine, 51*(31), 706–713. https://doi.org/10.1016/j.ifacol.2018.10.162

Vasudev, A., Cafari, A., Axelsson, M., Mikulski, M., & Hyvonen, J. (2022a). *SAE Technical Paper 2022-01-1033*. SAE Powertrains, Fuels & Lubricants Conference & Exhibition. https://doi.org/10.4271/2022-01-1033

Vasudev, A., Mikulski, M., Balakrishnan, P. R., Storm, X., & Hunicz, J. (2022b). Thermo-kinetic multi-zone modelling of low temperature combustion engines. *Progress in Energy and Combustion Science, 91*, Article 100998. https://doi.org/10.1016/j.pecs.2022.100998

Wärtsilä. (n.d.). *Wärtsilä UNIC engine control system for gas and dual fuel engines*. https://cdn.wartsila.com/docs/default-source/service-catalogue-files/electrical-automation-services/wartsila-unic-engine-control-system-for-gas-and-dual-fuel-engines.pdf?sfvrsn=94571e45_8.

Xia, L., Willems, R., Jager, B.de, & Willems, F (2019). Constrained optimization of fuel efficiency for RCCI engines. *IFAC-PapersOnLine, 52*(5), 648–653. https://doi.org/10.1016/j.ifacol.2019.09.103

Yao, T., Pei, Y., Zhong, B.-J., Som, S., Lu, T., & Luo, K. H. (2017). A compact skeletal mechanism for n-dodecane with optimized semi-global low-temperature chemistry for diesel engine simulations. *Fuel, 191*, 339–349. https://doi.org/10.1016/j.fuel.2016.11.083